Trajectory Investigations of the Dissociation Dynamics of Vinyl Bromide on an ab Initio Potential-Energy Surface

Asif Rahaman and Lionel M. Raff*

Department of Chemistry, Oklahoma State University, Stillwater, Oklahoma 74078

Received: May 4, 2000; In Final Form: July 31, 2000

The reaction dynamics of vibrationally excited vinyl bromide have been investigated using classical trajectory methods on a global, analytic potential-energy hypersurface that is developed primarily by least-squares fitting of appropriately chosen functional forms to the results of ab initio electronic structure calculations. These calculations are carried out at the MP4 level of theory with all single, double, and triple excitations included. A 6-31G(d,p) basis set is employed for the carbon and hydrogen atoms. Huzinaga's (4333/433/4) basis set augmented with split outer s and p orbitals (43321/4321/4) and a polarization f orbital with an exponent of 0.5 is used for the bromine atom. The present calculations focus upon the determination of the dependence of the potential upon the stretching coordinates for the bonded atoms in vinyl bromide, the C−C−H and C−C−Br bending coordinates and the dihedral angles. The couplings between these coordinates are also investigated. The total ab initio database is obtained by combining these results with previously reported studies of the vinylidene−acetylene system and our previous calculations of saddle-point geometries and energies for the various decomposition channels, reactant and product equilibrium structures, and vibrational frequencies. The analytic surface fitted to this data base (PES1) is then modified by adjustment of the potential curvatures at equilibrium to provide a better fit to the measured IR and Raman vibrational frequencies of vinyl bromide while simultaneously holding all other topographical features of the surface constant to the maximum extent possible. The surface so developed is labeled PES2. Finally, we have arbitrarily altered the reaction coordinate curvatures for three-center HBr and H_2 elimination to produce a third potential surface (PES3). The dissociation dynamics of vinyl bromide on each of these potential surfaces are investigated at several excitation energies in the range 4.5 to 6.44 eV. Total decomposition rate coefficients and product branching ratios are computed as a function of excitation energy. The HBr vibrational-state distribution is computed and found to be Boltzmann with an effective vibrational temperature of 7084 K on PES1. These results are in virtually exact agreement with recently reported measurements of this distribution. Finally, we have investigated the dissociation mechanisms for three-center H_2 and HBr elimination reactions. The results show that the dynamics are very similar on PES1, PES2, and PES3. Consequently, small variations in potential-energy curvatures at equilibrium and along the reaction coordinates do not exert significant influence upon the dissociation dynamics. However, some large qualitative variations between the dynamics on the ab initio surface and the more empirical surface previously employed are found to exist. We conclude that great care must be exercised when such surfaces are used to study reaction dynamics in polyatomic systems.

I. Introduction

Molecular dynamics (MD) simulations are the most powerful existing method for the investigation of dynamical behavior of atomic and molecular motions of complex systems. To date, such studies have been used to study chemical reaction mechanisms, energy transfer pathways, reaction rates, and product yields in a wide array of polyatomic systems. In addition, MD methods have been successfully applied to the investigation of gas−surface reactions, diffusion on surfaces and in the bulk, membrane transport, the synthesis of diamond using chemical vapor deposition techniques, nanometric machining and cutting, as well as scratching, grinding, and tensile properties. The structure of vapor deposited rare gas matrixes has been studied using trajectories procedures. With the advent of relatively inexpensive, powerful workstations, such calculations have become routine. Once the potential-energy hypersurface for the system has been obtained, the computation of a suitably large ensemble of trajectories is straightforward. In the majority of cases, the computation time required is on the order of hours to a few weeks.

The major problem associated with MD investigations is the development of a potential-energy surface whose topographical features are sufficiently close to those of the true, but unknown surface, that the results of the trajectories are experimentally meaningful. In the case of simple, three-body reactions such as $H + D_2 \rightarrow HD + D$ or the other possible isotopic analogues, very accurate surfaces have been computed using multiconfiguration ab initio methods.[1] For polyatomic reactions involving several competing reaction channels, the situation is much more uncertain. Investigators have generally resorted to the use of an ad hoc semiempirical surface fitted in some fashion to different types of experimental data related to the system to be studied. In other cases, the dimensionality of the potential hypersurface has been arbitrarily reduced to simplify the calculations.

It would be very helpful if extensive high-level ab initio potential surfaces could be obtained for a few, carefully selected polyatomic systems possessing several energetically open reac-

* To whom correspondence should be addressed. Fax: (405) 744−6007

10.1021/jp001695t CCC: $20.00
Published on Web 10/27/2000

tion channels. The objective of this research is the development of such a potential for the C_2H_3Br system. Comparison of the results of dynamical studies on this surface with those obtained from more approximate potential formulations would permit an accurate assessment of the relative importance of different topographical features of the potential and the degree of confidence that can be assigned to results obtained with more approximate potential surfaces.

II. Potential Surface Formulations in Polyatomic Systems

The calculation of a potential-energy surface for a polyatomic system is difficult primarily because the dimensionality of the surface generally precludes the possibility of high-level electronic structure calculations for a sufficiently large number of configurations to obtain a global representation of the surface that properly considers all open reaction channels. The fact that there have been hundreds of theoretical investigations of inelastic and reaction dynamics for three and four-body systems, but more than an order of magnitude fewer for systems containing five or more atoms is a reflection of the problems presented by polyatomic molecules.

The level of difficulty associated with obtaining global potentials has led to attempts to predict reaction mechanisms based on the relative energies of the surface's stationary points alone.[2] These points are often sufficiently few in number that accurate configuration interaction (CI) or fourth-order Möller−Plesset perturbation theory (MP4) calculations with large basis sets can be executed. By assuming that the favored reaction pathways correspond to the minimum-energy paths, reaction mechanisms can be inferred from the stationary-point energies without actually conducting trajectory or semiclassical scattering calculations on a global potential-energy surface. For thermal systems, this assumption is generally very accurate, but for reactions occurring at fixed-energies well above the potential barriers, the major reaction pathways often do not correspond to the minimum-energy paths.

Two studies that are particularly relevant to our research on the reaction dynamics of vinyl bromide involve the decomposition pathways of ethylene and vinyl chloride. Jensen, Morokuma, and Gordon[3] determined the C_2H_4 molecular geometries at the stationary points at the MP2 level with 6-31G(d,p) and 6-31G** basis sets. Energies at these points were obtained from MP4 calculations with G-311 + G(d,p) basis sets. The three-center H_2 dissociation channel leading to H_2 and vinylidene was found to have a barrier of 93.8 kcal mol^{-1}. No transition state could be located for a four-center elimination reaction. The mechanism involving a hydrogen-atom transfer to form ethylidene followed by a 1,1-H_2 elimination has a calculated barrier of 109.5 kcal mol^{-1}. Consequently, the predicted H_2 dissociation mechanism is an α,α process in agreement with the experimental observations reported by Okabe and McNesby[4] and by Balko et al.[5] Riehl and Morokuma[6] employed quadratic single and double CI methods which included a triple contribution with 6-31G(d,p) basis sets at geometries obtained from MP2 calculations to examine the mechanism for decomposition of vinyl chloride. The energetically favored pathway for decomposition is α,α HCl elimination, which has a computed barrier of 69.1 kcal mol^{-1}. The barrier for the corresponding α,β process is 77.4 kcal mol^{-1}. The α,α H_2 elimination has a 97.2 kcal mol^{-1} barrier. No transition state could be located for four-center H_2 dissociation. Consequently, the energetically favored decomposition channels are, in order of importance, α,α HCl elimination, and α,α H_2 elimination. These results are in accord with recent experiments[7−9] that show that the large majority of the HCl product is formed by three-center elimination.

Another approach that has been employed to develop global potentials for complex systems uses parametrized functional forms suggested by physical and chemical considerations to fit thermochemical, spectroscopic, structural, and kinetic data.[10] This empirical procedure generally appears to work well provided the critical potential barriers to reaction can be accurately estimated from measured activation energies. To date, the most successful approach is a combination of the above methods.[11] This "hybrid" technique involves the high-level ab initio computation of the transition-state geometries, frequencies, and energies. A global potential is then developed by making astute choices for the parametrized functional forms used to represent the important motions of the system. This potential is fitted to a database comprising the experimental thermochemical, spectroscopic, and structural data and all the ab initio data related to the transition states. Because this data base is much larger than that available from experimental data alone, it is reasonable to expect the global surfaces to be correspondingly more accurate.

We have employed such a hybrid method to obtain a global representation of the ground-state surface for the vinyl bromide system.[12] The equilibrium structures for vinyl bromide, bromoacetylene, the vinyl radical, the vinylidene radical, and the bromovinylidene radical were determined at the Hartree−Fock level using 6-31G(d,p) basis sets for carbon and hydrogen, and Huzinaga's (4333/433/4) basis set[13] augmented with split outer s and p orbitals (43321/4321/4) to improve the flexibility for bromine. To include a more accurate description of bromine atom polarization effects, additional calculations were carried out with the basis set modified to (43321/4321/4/1) by adding polarization f orbitals with the exponent 0.5. Dynamic correlation was taken into account at the MP4(SDTQ) level of theory using this basis set. These methods were also used to determine the transition-state structures, vibrational frequencies, and energies for three-center HBr and H_2 elimination and four-center HBr and H_2 elimination. These results were combined with ab initio studies of the vinylidene → acetylene potential barrier reported by Osamura et al.,[14] Krishnan et al.,[15] Smith et al.[16] and Halvick et al.[17] to form part of the database to which the global analytic surface was fitted. The remainder was obtained from experimentally measured heats of reaction, vibrational frequencies and equilibrium structures.

III. ab Initio Calculations

Because it is impossible to accurately compute the full 16-dimensional potential-energy hypersurface for the C_2H_3Br system, we have elected to concentrate our efforts on a determination of the dependence of the potential upon the stretching coordinates for the bonded atoms in vinyl bromide, the C−C−H and C−C−Br bending coordinates and variations of the dihedral angles. To obtain an accurate description of the reaction and energy transfer dynamics, we also need an evaluation of the effect upon the potential brought about by coupling between these coordinates.

As in our previous calculations on this system,[12] we have carried out ab initio calculations at the MP4(SDT) level of theory using the GAUSSIAN 94[18] package. For the carbon and hydrogen atoms, 6-31G(d,p) basis were employed. Huzinaga's[19] (4333/433/4) basis set augmented with split outer s and p orbitals (43321/4321/4) are used for the bromine atom. A polarization f orbital is added with an exponent of 0.5 to provide a more accurate description.

In all calculations, relaxed potential-energy scans for all bonds, angles, and dihedral angles were performed. Each bond

TABLE 1: Reaction Channels in the Decomposition of Vinyl Bromide[a]

channel label	reaction[b]	description
I	$C_2H_3Br \rightarrow C_2H_3 + Br$	bromine atom dissociation
IIA	$C_2H_3Br \rightarrow H^5Br + C_2H_2$	four-center HBr elimination
IIB	$C_2H_3Br \rightarrow H^5 + Br + C_2H_2$	four-center H + Br dissociation
IIIA	$C_2H_3Br \rightarrow H^4Br + C_2H_2$	four-center HBr elimination
IIIB	$C_2H_3Br \rightarrow H^4 + Br + C_2H_2$	four-center H + Br elimination
IVA	$C_2H_3Br \rightarrow H^3H^4 + HC{\equiv}CBr$	four-center H_2 elimination
IVB	$C_2H_3Br \rightarrow H^3 + H^4 + HC{\equiv}CBr$	four-center H+ H elimination
VA	$C_2H_3Br \rightarrow H^3H^5 + HC{\equiv}CBr$	four-center H_2 elimination
VB	$C_2H_3Br \rightarrow H^3 + H^5 + HC{\equiv}CBr$	four-center H+ H elimination
VI	$C_2H_3Br \rightarrow H^3Br + H_2C{=}C$	three-center HBr elimination
	$H_2C{=}C \rightarrow HC{\equiv}CH$	vinylidene to acetylene conversion
VII	$C_2H_3Br \rightarrow H^4H^5 + C{=}CHBr$	three-center H_2 elimination

[a] Each of these is described by the potential surface employed in the investigations reported in reference 1. [b] Superscripts give the atom numbers as defined in Figure 1.

is stretched or compressed in increments of 0.1 Å from its equilibrium value. At each increment, the C_2H_3Br system is relaxed by optimization of the geometry while keeping the bond distance under investigation fixed. In a similar manner, the three C−C−H angles and the C−C−Br angle are each varied from their equilibrium value in increments of five degrees. At each point, the geometry of the system is optimized while maintaining the angle under study fixed. Because variation of these angles along with three of the dihedral angles incorporates variations due to either the H−C−H or the H−C−Br angles, the effects of varying these angles upon the potential is indirectly included in the calculations.

The dihedral angles are all coupled. Therefore, it is impossible to compute the effect upon the potential of changing a single dihedral angle. Our procedure is to compute the total change in the potential as all four of the dihedral angles change upon torsional rotation of vinyl bromide using relaxed potential-energy scans in the same manner as that used to investigate the dependence of the potential upon bond lengths and angles. For purposes of fitting the resulting data to analytic functions for each dihedral angle, we assume that all dihedral interactions make equal contributions to the total potential energy. With this assumption, the ab initio energy variations are divided by four, because there are four dihedral angles involved, to obtain the contribution from each individual dihedral angle.

In the present study, the energy of 299 different nuclear conformations have been computed using the above methods. Because knowledge of the MP4 energies for each of these conformations is not required for understanding the principle conclusions of this investigation, the ab initio data are being submitted as Supporting Information. Combination of these results with previous ab initio computations of reactant, product and transition-state energies and geometries[12,14−17] gives us a database of about 400 points to which analytic functions can be fitted to produce an ab initio potential surface that we shall label as PES1. The analytical fitting of this data base is described in the next section.

IV. Analytical Fitting and Comparison to ab Initio Calculations

Our approach to fitting the results of ab initio electronic structure calculations is to develop analytic functions for each of the energetically open reaction channels using functional forms suggested by physical and chemical considerations. The "parameters" of these functions are expressed as appropriate functions of the system's geometry. These channel potentials are connected smoothly with parametrized switching functions that play a central role in fitting the potential barriers, reaction

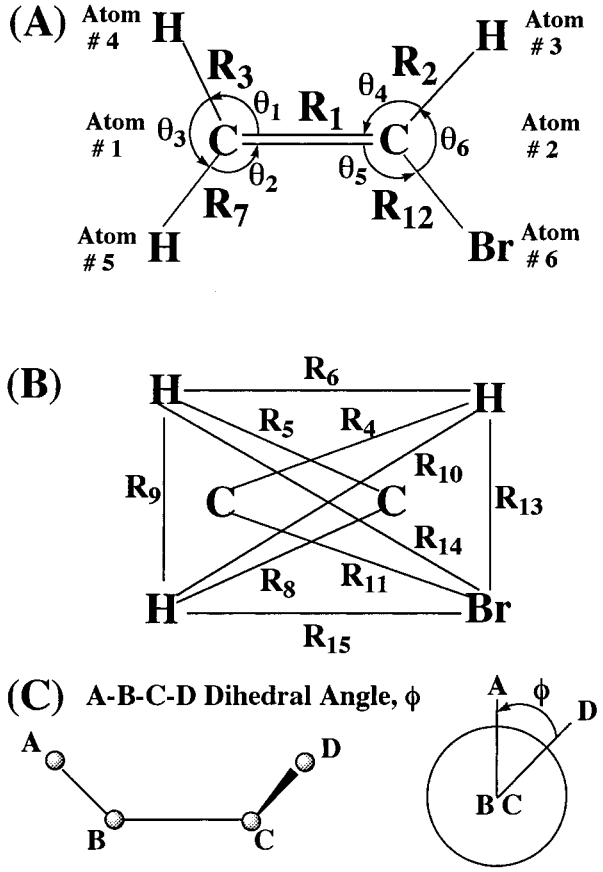

Figure 1. (A) Atom numbering, interatomic distance, and angle definitions for bonded atoms (B) Interatomic distance definitions for nonbonded atoms (C) Dihedral angles are defined as follows: $\phi_1 = H^4{-}C^1{-}C^2{-}H^3$; $\phi_2 = H^4{-}C^1{-}C^2{-}Br$; $\phi_3 = H^5{-}C^1{-}C^2{-}H^3$; $\phi_4 = H^5{-}C^1{-}C^2{-}Br$.

coordinate curvatures and coordinate coupling terms obtained in the ab initio calculations.

Figure 1 shows the labeling of atoms used throughout the description of the analytical potential fit and in the dynamics calculations. Figure 1A defines the interatomic distances for the bonded atoms. The interatomic distance definitions between nonbonded atoms are given in Figure 1B. Figure 1C defines the four dihedral angles employed in the analytic fitting of the ab initio database.

The reaction channels of primary interest in the decomposition of vinyl bromide are summarized in Table 1. Each of these reaction channels was open on the hybrid surface employed by Abrash et al.[12] to investigate the decomposition dynamics of vinyl bromide at energies 4.00 to 6.44 eV in excess of zero-

point energy. We shall denote this hybrid potential as EPS. The results of these studies indicate that at higher energies, the dissociation of vinyl bromide occurs primarily via three-center HBr elimination followed by three-center H_2 elimination, Br-atom dissociation, and H-atom dissociation. Four-center decomposition channels were found to play virtually no role in the decomposition dynamics. Consequently, our analytic fit to the ab initio database incorporates only the three-center and atom-dissociation channels.

The overall potential-energy function, V_T, for C_2H_3Br is written in terms of channel potentials as

$$V_T = [V_I S_3S_4S_5 + V_{VI} S_6] S_7S_8S_9 + V_{VII} S_{10} \quad (1)$$

where the S_i (i = 3, 4, 5, ..., 10) are the switching functions that smoothly connect the various channel potentials, V_I, V_{VI}, and V_{VII}. The notation for the channel potentials is chosen so as to be consistent with that employed by Abrash et al.[12] for the EPS potential. V_I describes vinyl bromide and the atom-dissociation channels leading to bromine or hydrogen-atom elimination. V_{VI} and V_{VII} describe the channels leading to three-center HBr and H_2 elimination, respectively. The switching functions are given by

$$S_3 = 1 - A_7A_{12}(1 - A_3)(1 - A_2) \quad (2)$$

$$S_4 = 1 - A_3A_{12}(1 - A_2)(1 - A_7) \quad (3)$$

$$S_5 = 1 - E_2E_{12} \quad (4)$$

$$S_6 = F_2F_{12} \quad (5)$$

$$S_7 = 1 - C_2C_7(1 - C_{12})(1 - C_3) \quad (6)$$

$$S_8 = 1 - C_2C_3(1 - C_{12})(1 - C_7) \quad (7)$$

$$S_9 = 1 - G_3G_7 \quad (8)$$

and

$$S_{10} = H_3H_7 \quad (9)$$

In the above definitions, the subscripts on A, C, E, F, G, and H indicate the dependence of these functions upon the corresponding interatomic distance defined in Figure 1. The A_i (i = 2, 3, 7, or 12) all have the form

$$A_i = A_i(R_i; a_i, R_i^o) = \tanh[\exp\{a_i(R_i - R_i^o)^2\} - 1] \quad (10)$$

where a_i and R_i^o are parameters characteristic of the particular A_i function. The remaining C, E, F, G, and H functions have the form

$$T_i(R_i; a_i, R_i^o) = \tanh[a_i(R_i - R_i^o)^2\}] \quad (T_i = C_i, E_i, F_i, G_i, \text{or } H_i) \quad (11)$$

The R_i^o parameters are the ground-state equilibrium bond lengths and the a_i are parameters used to fit the potential barriers predicted by the ab initio calculations[12] for the various reaction channels. In all cases, we have $a_i > 0$. The values of these parameters obtained from the least-squares fitting are listed in Table 2.

Examination of eqs 10, 11, and 1 shows that when we have all the interatomic distances of the bonded atoms in vinyl bromide at or near their equilibrium values, the values of all the A, C, E, F, G, and H functions approach zero. This gives the result S_3, S_4, S_5, S_7, S_8, $S_9 \rightarrow 1$ and S_6, $S_{10} \rightarrow 0$, so that the system potential approaches V_I that accurately describes vinyl bromide. When hydrogen atom 3 on carbon atom 2 dissociates in an atomic hydrogen-atom elimination reaction while the remaining interatomic distances remain near their equilibrium values, we have all A, C, E, F, G, and H functions approaching zero except for A_2, C_2, and F_2, which approach unity. Under this condition, we again find that S_3, S_4, S_5, S_7, S_8, $S_9 \rightarrow 1$, and S_6 and $S_{10} \rightarrow 0$, so that the system potential again approaches V_I, which describes the atomic dissociation channels. A similar result is obtained if we examine the limits for dissociation of hydrogen atoms 4 or 5 and for Br-atom elimination. In contrast, if three-center elimination of H^3Br (H^3 denotes hydrogen atom number three in Figure 1) occurs, all A, C, E, F, G, and H functions with either a subscript 2 or 12 will approach unity while all others approach zero. This produces the result S_3, S_4, S_6, S_7, S_8, $S_9 \rightarrow 1$ while S_5 and $S_{10} \rightarrow 0$. Therefore, the total potential approaches the channel potential V_{VI} that describes three-center HBr elimination. A similar analysis shows that three-center elimination of H^4H^5 causes the system potential to approach V_{VII}. Consequently, eq 1 possesses the correct asymptotic behavior to describe the important reaction channels. The critical point is to properly adjust the parameters to produce accurate fits of the ab initio data base.

TABLE 2: Switching Function Parameters for the Fit to the ab Initio Calculations, Surface PES1, and Surfaces PES2 and PES3

	PES1		PES2		PES3	
function	a_i (Å^{-2})	R_i^o (Å)	a_i (Å^{-2})	R_i^o (Å)	a_i (Å^{-2})	R_i^o (Å)
A_2	5.00	1.0785	5.00	1.0785	5.00	1.0785
A_3	5.00	1.0811	5.00	1.0811	5.00	1.0811
A_7	5.00	1.0803	5.00	1.0803	5.00	1.0803
A_{12}	5.00	1.9229	5.00	1.9229	5.00	1.9229
C_2	7.825	1.0785	7.825	1.0785	7.825	1.0725
C_3	7.825	1.0811	7.825	1.0811	7.825	1.0811
C_7	7.825	1.0803	7.825	1.0803	7.825	1.0803
C_{12}	7.500	1.9229	7.500	1.9229	7.500	1.9229
E_2	6.700	1.0785	3.900	1.0785	3.900	1.0785
E_{12}	6.700	1.9229	3.900	1.9229	3.900	1.9229
F_2	7.500	1.0785	5.500	1.0785	5.900	1.0785
F_{12}	7.000	1.9229	4.050	1.9229	4.050	1.9229
G_3	7.820	1.0811	7.820	1.0811	7.200	1.0811
G_7	7.820	1.0803	7.820	1.0803	7.200	1.0803
H_3	8.578	1.0811	8.918	1.0811	9.300	1.0811
H_7	8.058	1.0803	7.878	1.0803	8.478	1.0803

The Channel I potential, V_I, represents the system when its configuration corresponds to either reactant, product or transition state for vinyl bromide undergoing Br or H-atom dissociation. It is written as a sum of stretching potentials for bonds, bending potentials for angles and torsional potentials for the dihedral angles

$$V_I = V_{CC} + V_{CBr} + V_{CH^3} + V_{CH^4} + V_{CH^5} + \sum_{i=1}^{6} V_i(\theta_i) + \sum_{i=1}^{4} V_{ABCD}(\phi_i) \quad (12)$$

where $V_i(\theta_i)$ is a three-body bending potential for the angle θ_i. The last term in eq 12 sums the dihedral potentials for the dihedral angles ϕ_i (i = 1, 2, 3, or 4) formed by $H^4-C-C-H^3$, $H^4-C-C-Br$, $H^5-C-C-H^3$, and $H^5-C-C-Br$, respectively. These angles are defined in Figure 1C.

TABLE 3: Stretching Potential Parameter Values for Surface Fits PES1, PES2, and PES3

bonded atoms					bonded atoms				
i	*j*	parameter	PES1	PES2 and PES3	*i*	*j*	parameter	PES1	PES2 and PES3
C	C	$D_{ij}^{(4)}$	5.197 eV	5.197 eV	C	H^4	$D_{ij}^{(4)}$	4.876 eV	4.876 eV
		$D_{ij}^{(1)}$	4.959 eV	4.959 eV			$D_{ij}^{(1)}$	4.876 eV	4.876 eV
		$\alpha_{ij}^{(4)}$	2.350 Å^{-1}	2.350 Å^{-1}			$\alpha_{ij}^{(4)}$	1.990 Å^{-1}	1.990 Å^{-1}
		$\alpha_{ij}^{(1)}$	2.500 Å^{-1}	2.180 Å^{-1}			$\alpha_{ij}^{(1)}$	2.000 Å^{-1}	1.775 Å^{-1}
		$R_{ij}^{(4)}$	1.342 Å	1.342 Å			$R_{ij}^{(4)}$	1.105 Å	1.105 Å
		$R_{ij}^{(1)}$	1.3307 Å	1.3035 Å			$R_{ij}^{(1)}$	1.0811 Å	1.0811 Å
		β_{ij}	0.521 08 (eV Å^{-1})	0.521 08 (eV Å^{-1})			β_{ij}	0.124 09 (eV Å^{-1})	0.124 09 (eV Å^{-1})
		λ_{ij}	5.280 36 (eV)	5.227 18 (eV)			λ_{ij}	3.719 96 (eV)	3.500 72 (eV)
		μ_{ij}	5.121 42 (eV A^{-1})	4.075 08 (eV Å^{-1})			μ_{ij}	0.748 08 (eV A^{-1})	0.231 77 (eV Å^{-1})
		R_{ij}^{c}	1.60 Å	1.60 Å			R_{ij}^{c}	2.00 Å	2.00 Å
		c_1	0.400 (Å^{-2})	0.400 (Å^{-2})			c_1	0.400 (Å^{-2})	0.400 (Å^{-2})
		c_2	1.9229 (Å)	1.9229 (Å)			c_2	1.9229 Å	1.9229 Å
C	Br	$D_{ij}^{(4)}$	3.339 eV	3.339 eV	C	H^5	$D_{ij}^{(4)}$	4.876 eV	4.876 eV
		$D_{ij}^{(1)}$	3.339 eV	3.339 eV			$D_{ij}^{(1)}$	4.876 eV	4.876 eV
		$\alpha_{ij}^{(4)}$	1.459 Å^{-1}	1.599 Å^{-1}			$\alpha_{ij}^{(4)}$	1.990 Å^{-1}	1.990 Å^{-1}
		$\alpha_{ij}^{(1)}$	1.459 Å^{-1}	1.599 Å^{-1}			$\alpha_{ij}^{(1)}$	2.000 Å^{-1}	1.775 Å^{-1}
		$R_{ij}^{(4)}$	1.9229 Å	1.9229 Å			$R_{ij}^{(4)}$	1.099 Å	1.099 Å
		$R_{ij}^{(1)}$	1.9229 Å	1.9229 Å			$R_{ij}^{(1)}$	1.0803 Å	1.0803 Å
		β_{ij}	0.428 46 (eV Å^{-1})	0.428 26 (eV Å^{-1})			β_{ij}	0.372 47 (eV Å^{-1})	0.372 47 (eV Å^{-1})
		λ_{ij}	3.690 15 (eV)	4.224 12 (eV)			λ_{ij}	4.637 33 (eV)	4.411 36(eV)
		μ_{ij}	1.110 67 (eV A^{-1})	2.070 47 (eV Å^{-1})			μ_{ij}	2.295 98 (eV A^{-1})	1.307 61 (eV Å^{-1})
		R_{ij}^{c}	3.00 Å	3.00 Å			R_{ij}^{c}	2.00 Å	2.00 Å
		c_1	0.400 (Å^{-2})	0.400 (Å^{-2})			c_1	0.400 (Å^{-2})	0.400 (Å^{-2})
		c_2	1.9229 Å	1.9229 Å			c_2	1.9229 Å	1.9229 Å
C	H^3	$D_{ij}^{(4)}$	4.876 eV	4.876 eV					
		$D_{ij}^{(1)}$	4.876 eV	4.876 eV					
		$\alpha_{ij}^{(4)}$	2.000 Å^{-1}	1.775 Å^{-1}					
		$\alpha_{ij}^{(1)}$	1.981 Å^{-1}	1.981 Å^{-1}					
		$R_{ij}^{(4)}$	1.097 Å	1.097 Å					
		$R_{ij}^{(1)}$	1.0785 Å	1.0785 Å					
		β_{ij}	0.317 71 (eV Å^{-1})	0.317 71 (eV Å^{-1})					
		λ_{ij}	4.440 46 (eV)	4.212 23 (eV)					
		μ_{ij}	1.954 33 (eV A^{-1})	0.963 50 (eV Å^{-1})					
		R_{ij}^{c}	2.00 Å	2.00 Å					
		c_1	0.400 (Å^{-2})	0.400 (Å^{-2})					
		c_2	1.9229 Å	1.9229 Å					

The first five terms in eq 12 are the bond stretching potentials for the five chemical bonds in vinyl bromide that we wish to fit to the ab initio database for these bonds. Empirical examination of several possible fitting functions have led us to the following choices for these functions

$$V_{ij}(R_{ij}) = D_{ij}[\exp\{-2\alpha_{ij}(R_{ij} - R_{ij}^{o})\} - 2\exp\{-\alpha_{ij}(R_{ij} - R_{ij}^{o})\}] + \beta_{ij}(R_{ij} - R_{ij}^{o}) \text{ for } R_{ij} \le R_{ij}^{c} \quad (13)$$

and

$$V_{ij}(R_{ij}) = [\lambda_{ij} - \mu_{ij}(R_{ij} - R_{ij}^{o})]\exp\{-(R_{ij} - R_{ij}^{o})^2\} \text{ for } R_{ij} \ge R_{ij}^{c} \quad (14)$$

In eq 13, D_{ij}, α_{ij}, and R_{ij}^{o} are functionally dependent upon the C−Br distance, R_{12}. This dependence is given by

$$D_{ij} = D_{ij}^{(4)} + [D_{ij}^{(1)} - D_{ij}^{(4)}]\,S_1(R_{12}) \quad (15)$$

$$\alpha_{ij} = \alpha_{ij}^{(4)} + [\alpha_{ij}^{(1)} - \alpha_{ij}^{(4)}]\,S_1(R_{12}) \quad (16)$$

and

$$R_{ij}^{o} = R_{ij}^{(4)} + [R_{ij}^{(1)} - R_{ij}^{(4)}]\,S_1(R_{12}) \quad (17)$$

The λ_{ij}, μ_{ij}, and β_{ij} parameters are fitted to the ab initio data subject to the constraint that the potentials and first derivatives given by eq 13 match those of eq 14 at the point $R_{ij} = R_{ij}^{c}$. The switching function $S_1(R_{12})$ varies the bond dissociation energy, the equilibrium separation and the equilibrium curvature of the $i-j$ bond as the bromine atom dissociates so that variations in these quantities as vinyl bromide converts to the vinyl radical can be properly represented. Its functional form is taken to be

$$S_1(R_{12}) = 1.00 - \tanh[c_1(R_{12} - c_2)^2] \quad (18)$$

With this definition, it is clear that the quantities $D_{ij}^{(1)}$, $\alpha_{ij}^{(1)}$, and $R_{ij}^{(1)}$ are the well depth, equilibrium curvature, and distance parameters for vinyl bromide, whereas $D_{ij}^{(4)}$, $\alpha_{ij}^{(4)}$, and $R_{ij}^{(4)}$ are the corresponding parameters for the vinyl radical. The fitted parameter values for all bonded atoms are given in Table 3.

Figure 2, parts A through E, shows comparisons of the bond potentials for C═C, C−Br, C−H^3, C−H^4, and C−H,[5] respectively, given by eqs 13−18 with the MP4 calculations described in the previous section. In each case, the curves are the results of nonlinear least-squares fitting of eqs 13−18 to the ab initio data, which are shown as solid points after shifting the equilibrium potential energy to zero and subtracting the bond dissociation energy from the computed values. For interatomic distances less than R_{ij}^{c}, the fits are seen to be very good. When $R > R_{ij}^{c}$, the electronic structure calculations yield energies that lie slightly above our fitted potentials because the molecular

orbital calculations overemphasize the importance of ionic terms. The MP4 data points to which eqs 13 and 14 are fitted are given in Tables 1S−5S in the Supporting Information.

The angular terms in eq 12, $\sum_i^6 V_i(\theta_i)$, represent the bending potentials for the six, three-body angles θ_i defined in Figure 1. The analytic fitting functions used for these potentials have the form

$$V_i(\theta_i) = 0.5\, k_i[\theta_i - \theta_i^o]^2 \quad (19)$$

where

$$k_i = k_i^o\, S_2(R_v) \quad (20)$$

with

$$S_2(R_v) = 1.0 - \tanh[a_{3i}(R_v - R_v^o)^2] \quad \text{for } (i = 1, 2, \text{or } 4) \quad (21A)$$

and

$$S_2(R_v) = 1.0 - \tanh[a_{3i}(R_v - R_v^o)] \text{ for } (i = 5) \quad (21B)$$

In eq 21, parts A and B, R_v is the interatomic distance other than C═C forming the angle θ_i in vinyl bromide and R_v^o is the corresponding equilibrium bond distance. The $S_2(R_v)$ function attenuates the bending potentials as R_v becomes large. Consequently, this function couples the stretching motions of vinyl bromide to the bending motions. It has been found that the ab initio data base can be adequately fitted using the angular bending terms for the three C−C−H angles and the C−C−Br angles. Consequently, only the $V_i(\theta_i)$ terms for θ_1, θ_2, θ_4, and θ_5 appear in PES1.

We incorporate variations in the vibrational force constants and equilibrium angles as vinyl bromide converts to the vinyl radical using the $S_1(R_{12})$ switching function in a manner analogous to that employed for stretching potentials in eqs 15 − 17. That is, we define these quantities to be

$$k_i^o = k_{i+6} + (k_i - k_{i+6})\, S(R_{12})\ (i = 1, 2,3,... 6) \quad (22)$$

and

$$\theta_i^o = \Theta_{i+6} + (\Theta_i - \Theta_{i+6})\, S(R_{12})\ (i = 1,2, 3,...6) \quad (23)$$

Consequently, k_i and Θ_i are the bending force constants and equilibrium angle, respectively, for angle θ_i in vinyl bromide and k_{i+6} and Θ_{i+6} are the corresponding constants for the vinyl radical. The values of k_i and Θ_i are fitted using least-squares methods to the ab initio data obtained in the electronic structure calculations. The k_{i+6} and Θ_{i+6} values are taken from our previous fitting[12] for the vinyl radical. The bending potential parameters are given in Table 4.

Figure 3, parts A through D, shows comparisons of the angular potentials, $V_i(\theta_i)$, for (i = 1,2, 4, 5), which are the C−C−H[3], C−C−H,[4] C−C−H[5], and C−C−Br angles, respectively, with the MP4 calculations described in the previous section. In each case, the curves are the results of nonlinear least-squares fitting to the ab initio data, which are shown as solid points after shifting the equilibrium potential energy to zero. At angles less than the equilibrium angle, the analytic potentials lie slightly below those given by the MP4 calculations. When the angle exceeds the equilibrium angle, the inequality is reversed. In general, the accuracy of the fits is very good.

TABLE 4: Bending Potential Parameter Values for V_I

	potential surface	
parameter	PES1	PES2/PES3
k_1	4.822 70	5.304 970 (eV rad^{-2})
k_2	4.937 56	5.875 696 (eV rad^{-2})
k_3	0.000 00	0.450 370 (eV rad^{-2})
k_4	5.012 50	3.308 250 (eV rad^{-2})
k_5	6.820 44	6.615 827 (eV rad^{-2})
k_6	0.000 00	0.000 000 1 (eV rad^{-2})
k_7	3.800 00	3.800 000 (eV rad^{-2})
k_8	3.800 00	3.800 000 (eV rad^{-2})
k_9	2.450 00	2.450 000 (eV rad^{-2})
k_{10}	4.600 00	4.600 000 (eV rad^{-2})
k_{11}	6.820 44	6.615 827 (eV rad^{-2})
k_{12}	0.000 00	0.000 000 1 (eV rad^{-2})
Θ_1	2.086 00	2.086 00 (rad)
Θ_2	2.134 00	2.134 00 (rad)
Θ_3	2.058 34	2.058 34 (rad)
Θ_4	2.157 00	2.157 00 (rad)
Θ_5	2.160 00	2.160 00 (rad)
Θ_6	1.960 72	1.960 72 (rad)
Θ_7	2.122 32	2.122 32 (rad)
Θ_8	2.127 56	2.127 56 (rad)
Θ_9	2.033 31	2.033 31 (rad)
Θ_{10}	2.363 18	2.363 18 (rad)
Θ_{11}	2.160 00	2.160 00 (rad)
Θ_{12}	1.960 72	1.960 72 (rad)
a_{31}	0.400 00	0.400 00 (rad^{-2})
a_{32}	0.750 00	0.750 00 (rad^{-2})
a_{33}	0.400 00	0.400 00 (rad^{-2})
a_{34}	0.450 00	0.450 00 (rad^{-2})
a_{35}	1.000 00	1.000 00 (rad^{-2})
a_{36}	1.000 00	1.000 00 (rad^{-2})

Tables 6S−9S in the Supporting Information give the MP4 energies to which the analytic surface is fitted.

The couplings between the stretching and bending coordinates have been determined using the MP4 calculations by evaluation of changes in the bending potential as a function of R_v. At fixed values of R_v with the corresponding angle θ_i at equilibrium, the remaining geometry of the molecule is optimized and the MP4 energy (E_i) is calculated. With the same optimized geometry, θ_i is changed by a small increment $\Delta\theta$ and the new energy (E_f) is computed. Equations 19 and 20 show that the difference in these two energies is given by

$$V(\theta_i^o + \Delta\theta) - V(\theta_i^o) = E_f - E_i = 0.5\, k_i^o\, S_2(R_v)[\Delta\theta]^2 \quad (24)$$

The same calculations with $R_v = R_v{}^o$ give

$$V(\theta_i^o + \Delta\theta) - V(\theta_i^o) = E_f^{eq} - E_i^{eq} = 0.5\, k_i^o\, S_2(R_v^o)[\Delta\theta]^2 = 0.5\, k_i^o\, [\Delta\theta]^2 \quad (25)$$

because $S_2(R_v{}^o) = 1$. Division of eq 24 by eq 25 gives

$$S_2(R_v) = \frac{E_f - E_i}{E_f^{eq} - E_i^{eq}} \quad (26)$$

The a_{3i} parameters in eq 21, parts A and B, are computed by least-squares fitting to the data points obtained using eq 26. The results are given in Table 4. Figure 4, parts A−D, compares the analytic $S_2(R_v)$ coupling function to the ab initio data, which are given by the points. Tables 10S−13S in the Supporting Information give the results of the MP4 calculations used in this fitting.

The $V_{ABCD}(\phi_i)$ terms in eq 12 represent the contributions from torsional variations in the vinyl bromide structure. These interactions are expressed in terms of four dihedral angles ϕ_i (i

TABLE 5: Potential Parameters for the Dihedral Interactions in the V_I Channel Potential

	value	
parameter	PES1	PES2/PES3
d_o	0.3325	0.3325 eV
d_1	0.0	0.0 eV
d_2	−0.4025	−0.4025 eV
d_3	0.0	0.0 eV
d_4	0.10275	0.10275 eV
d_5	0.0	0.0 eV
d_6	−0.03275	−0.03275 eV
Δ_1	1.000	1.000 eV
Δ_2	1.000	1.000 eV
Δ_3	1.000	1.000 eV
Δ_4	1.000	1.000 eV
Δ_5	1.100	1.100 eV
Δ_6	0.000	0.000
Δ_7	0.000	0.000
Δ_8	1.100	1.100 eV
b_{21}	0.130	0.130 Å^{-1}
b_{23}	0.220	0.220 Å^{-1}
b_{31}	0.500	0.500 Å^{-1}
b_{32}	0.500	0.500 Å^{-1}
b_{73}	0.160	0.160 Å^{-1}
b_{74}	0.250	0.250 Å^{-1}
$b_{12,2}$	0.550	0.550 Å^{-1}
$b_{12,4}$	0.550	0.550 Å^{-1}
F_1	1.000	0.580
F_2	1.000	0.890
F_3	1.000	0.980
F_4	1.000	0.850

$= 1, 2, 3, 4$) formed by atoms A, B, C and D as defined in Figure 1C. The analytic functions chosen to fit the energies obtained in the MP4 calculations have the form

$$V_{ABCD}(\phi_i) = V_i^o\, S_{3i}(R_{AB})\, S_{3i}(R_{CD})\, F_i\, \mathrm{Sum}(\phi_i) \qquad (27)$$

where

$$V_i^o = \Delta_{i+4} + (\Delta_i - \Delta_{i+4})\, S_1(R_{12}) \qquad (28)$$

and

$$\mathrm{Sum}(\phi_i) = \sum_{j=0}^{6} d_j \cos(j\phi_i) \qquad (29)$$

The values of d_j ($j = 0, 1, 2, 3,...6$) and Δ_i ($i = 1, 2, 3, 4$) are fitted to the energies obtained in the MP4 calculations. The Δ_{i+4} ($i = 1, 2, 3, 4$) parameters control the magnitude of the dihedral interactions in the vinyl radical. These values are taken from our previous formulation of the C_2H_3Br surface.[12] The F_i parameters introduce additional flexibility in the adjustment of the curvatures of the dihedral potential.

The $S_{3i}(R_{AB})$ and $S_{3i}(R_{CD})$ functions couple the dihedral interactions and the stretching coordinates for the A−B and C−D bonds. The general analytic form chosen for these functions is

$$S_{3i}(R_v) = 1.0 - \tanh[b_{vi}\,(R_v - R_v^o)] \qquad (30)$$

where R_v is either R_{AB} or R_{CD} as defined in Figure 1C, and R_v^o is the corresponding equilibrium distance for the A−B or C−D bond. The values of the b_{vi} parameters are obtained by least-squares fitting to the ab initio database as described below. The results of this fitting are given in Table 5. It should be noted that eq 30 ensures that the dihedral interactions vanish whenever either R_{AB} or R_{CD} become large.

Figure 5 compares the torsional potential given by eqs 27−29 with the results of the MP4 calculations for vinyl bromide with the interatomic distances between all bonded atoms and the bond angles, θ_i ($i = 1, 2, 3, ...,6$), fixed at their equilibrium values. As can be seen, the fit is excellent except at the point $\phi = 90°$, where the analytic fit underestimates the magnitude of the torsional barrier by about a 0.1 eV. The ab initio energies plotted in Figure 5 are given in Table 14S of the Supporting Information.

The parameters in the $S_{3i}(R_v)$ coupling functions are fitted to the MP4 calculations in a manner analogous to that described by eqs 24−26 for the S_2 functions. With vinyl bromide in its equilibrium conformation, the MP4 energy of system (E_i^{eq}) is computed. One of the dihedral angles (ϕ_1, ϕ_3, or ϕ_4) is then changed by 5° and the new system energy, (E_f^{eq}), is calculated. The bond distance R_v is now varied to a new value and the above calculations are repeated to obtain E_i and E_f for the new value of R_v. The value of $S_{3i}(R_v)$ predicted by the MP4 calculations is obtained using eq 26 with $S_2(R_v)$ replaced with $S_{3i}(R_v)$. The b_{vi} parameters in eq 30 are fitted to these data points using least-squares methods. Figure 6, parts A−F, shows comparisons of the ab initio results for $S_{3i}(R_v)$ with the analytic fits given by eq 30. Tables 15S−20S in the Supporting Information give the MP4 results used in the calculations.

The product configuration spaces for the three-center dissociation channels leading to HBr + $H_2C{=}C$ and H_2 + $C{=}CHBr$ are described by V_{VI} and V_{VII}, respectively. The V_{VI} potential has the form

$$V_{VI} = V_{HBr}(R_{13}) + V_{C_2H_2}(R_1,R_3,R_5,R_7,R_8) \qquad (31)$$

where $V_{HBr}(R_{13})$ is a simple Morse potential for HBr and $V_{C_2H_2}$ (R_1,R_3,R_5,R_7,R_8) is the vinylidene/acetylene potential, which has been previously fitted[12] to the results of ab initio electronic structure calculations.[14−17] The V_{VII} potential is

$$V_{VII} = V_{HH}(R_9) + V_{HBrC=C}(R_1,R_2,R_4,R_{11},R_{12}) \qquad (32)$$

$V_{HH}(R_9)$ is a Morse potential for H_2. The $V_{HBrC=C}(R_1,R_2,R_4,R_{11},R_{12})$ term is fitted to electronic structure results.[14−17] The complete details of the fitting for the product spaces of the three-center elimination channels are given in ref 12.

The foregoing discussion completes the description of potential surface PES1. To investigate the effects of equilibrium and reaction coordinate curvature upon the computed energy transfer and unimolecular dissociation dynamics of vinyl bromide, we have developed two additional potentials surfaces that alter these topographical features one at a time. Potential surface PES2 alters some of the parameters contained PES1 to obtain close agreement between the experimental and computed normal mode vibrational frequencies. These parameters include the α_{ij}, λ_{ij}, and μ_{ij} for the stretching terms, the k_i and k_{i+6} for the bending potentials, the F_i for the dihedral terms and a few of the switching function a_i parameters to maintain the potential barriers for the various reaction channels unaltered. We also incorporate an additional angular term for the H−C−H bend in the $\sum_{i=1}^{6} V_i(\theta_i)$ summation contained in eq 12. This addition permits us to obtain better agreement between theory and experiment for the low-frequency vibrations. An alternative procedure to fitting the measured scalar frequencies involves fitting the second derivatives of the potential at equilibrium. Such methods have been previously discussed by Dasgupta and Goddard[20] and by Rice et al.[21] This type of fitting is more demanding in that there are many more second derivatives than frequencies.

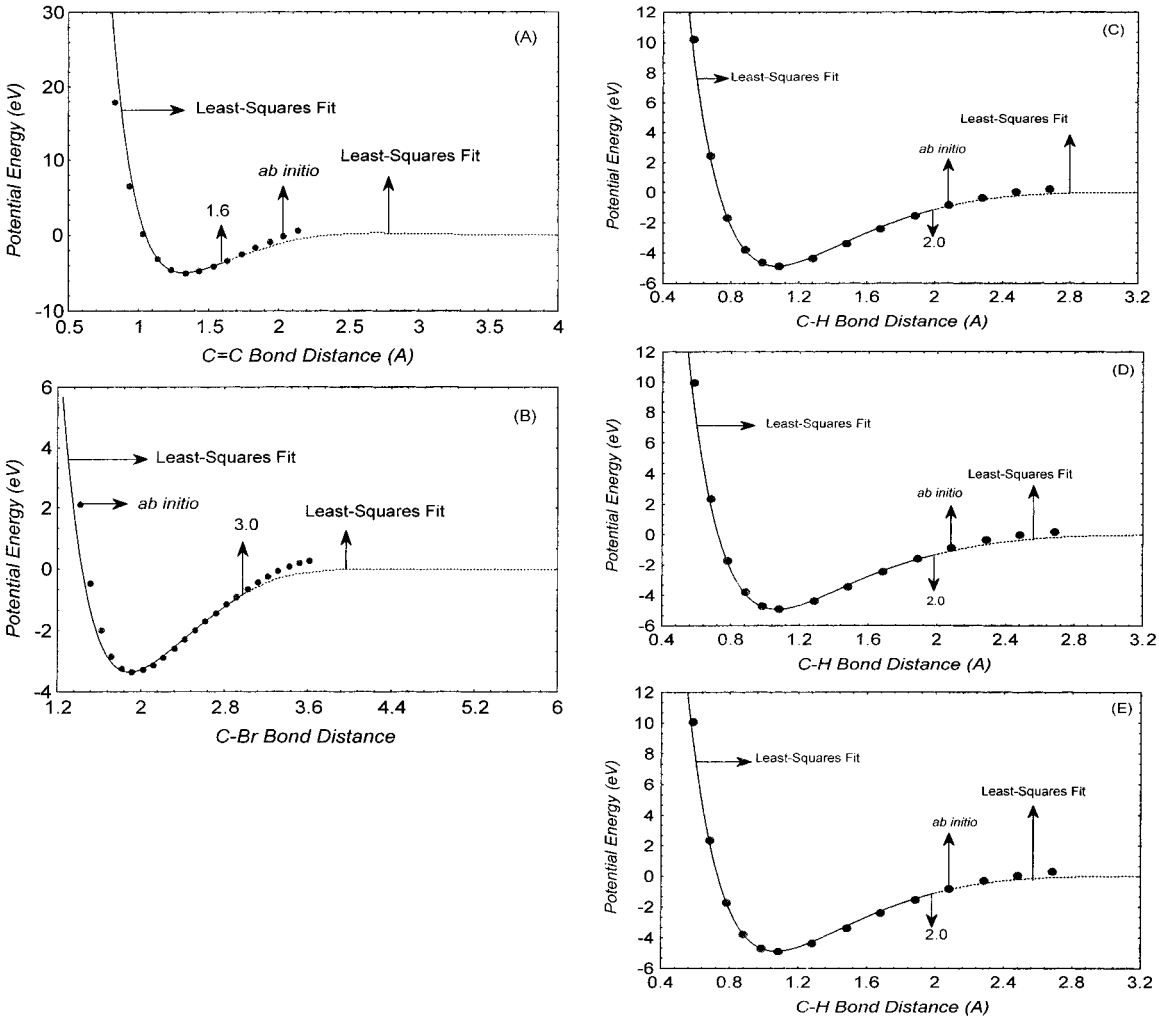

Figure 2. Stretching potentials for bonded atoms in the Channel I potential. The analytic fit to the MP4 data is shown as the curve. The switchover point at $R_{ij} = R_{ij}^c$ is indicated in the figures. The points are computed MP4 energies as described in the text. (A) C═C bond, (B) C−Br bond, (C) C−H^3 bond, (D) C−H^4 bond (E) C−H^5 bond.

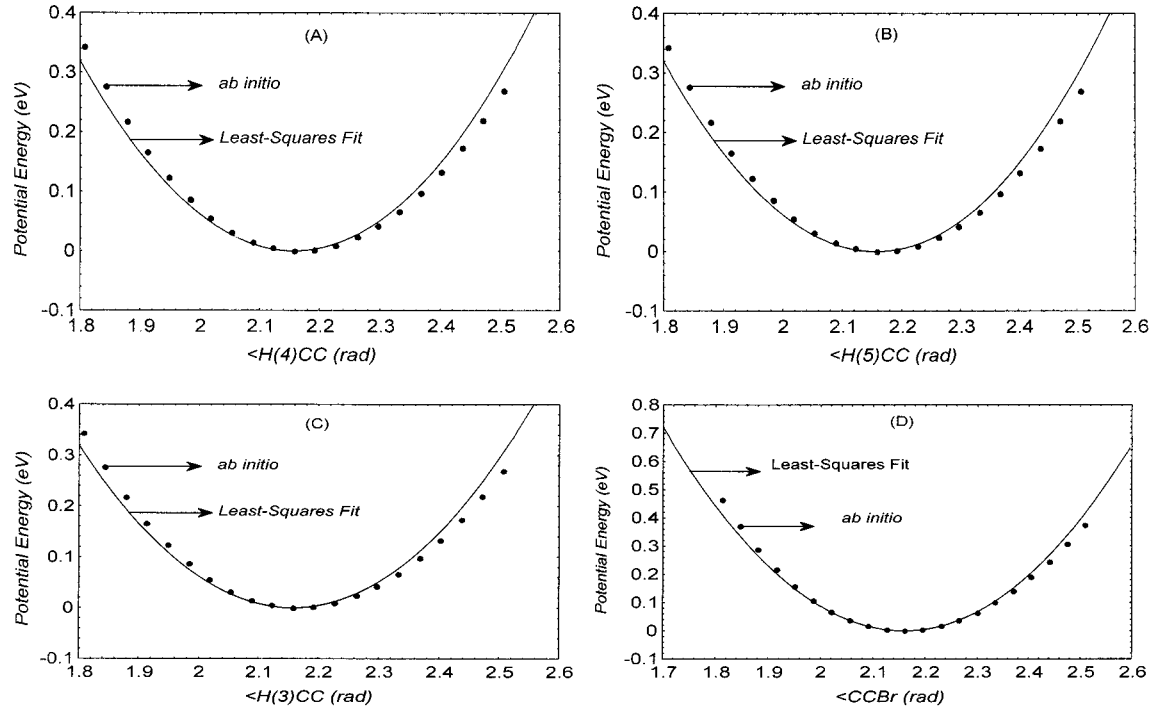

Figure 3. Angular potentials in the Channel I potential. The analytic fit to the MP4 data is shown as the curve. The points are computed MP4 energies as described in the text. (A) C−C−H^3 angle, (B) C−C−H^4 angle, (C) C−C−H^5 angle, (D) C−C−Br angle.

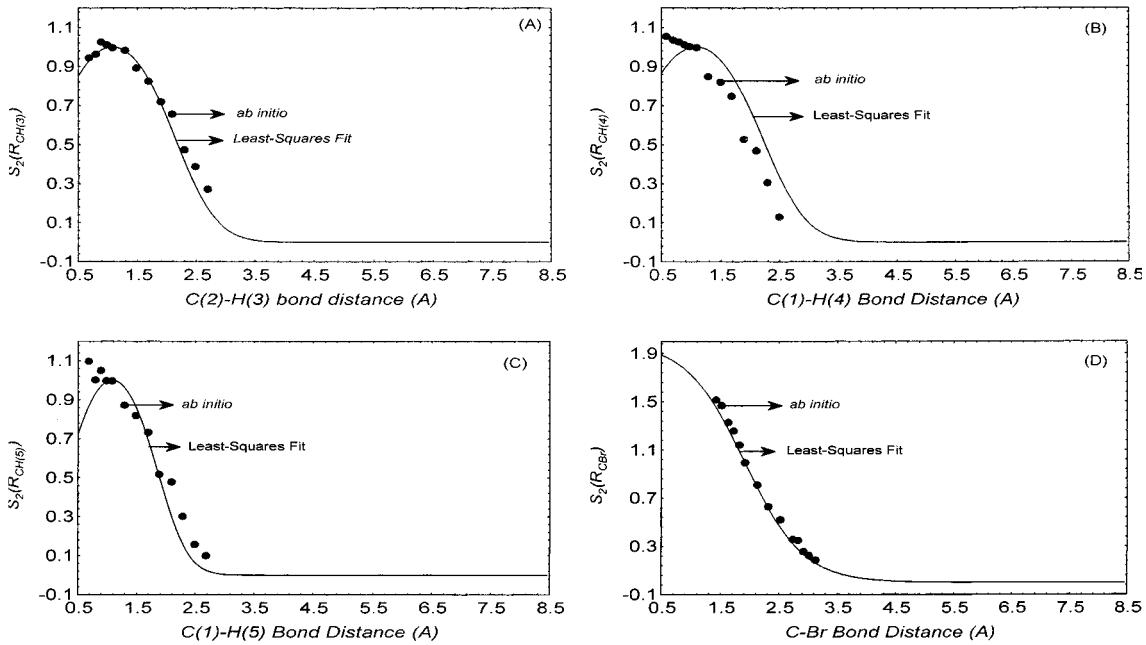

Figure 4. Variation of the $S_2(R_v)$ function defined by eq 26 for the C−C−X (X = H[3], H,[4] H[5], or Br) angle as a function of the C−X interatomic distance. The points are the results obtained in the MP4 calculations. The curve is a least-squares fit of eq 21A and 21B to these data. (A) C−C−H[3] angle, (B) C−C−H[4] angle, (C) C−C−H[5] angle, (D) C−C−Br angle.

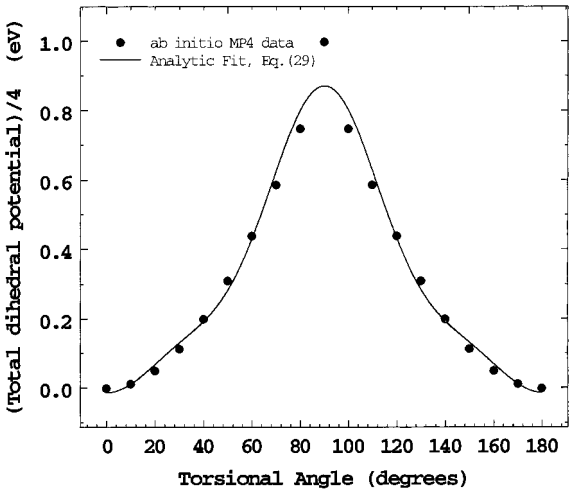

Figure 5. Comparison of the dihedral potential given by eqs 27−29 with the MP4 results obtained in the electronic structure calculations. The curve gives the analytic fit to the ab initio data that are shown as points. The ab initio energies are obtained by dividing the computed total torsional potential by four because four dihedral angles are changing as the torsional angle varies.

The effects upon the energy transfer and reaction dynamics introduced by alterations of the reaction coordinate curvatures and geometries have been investigated by developing a modification of PES2 that maintains all other topographical features nearly constant as these reaction coordinate properties are altered by varying primarily the switching function a_i parameters. Except for this constraint, the actual variations incorporated are arbitrary. We label this surface PES3.

The parameter values for surfaces PES2 and PES3 are given in Tables 2, 3, 4, and 5. An examination of these tables shows that most of the surface parameters for PES1 remain unchanged for PES2 and PES3.

V. Overview and Properties of the Potential Surfaces

Although we have termed surface PES1 an "ab initio" potential, it is clear that it is actually a hybrid between a pure ab initio surface and one that is semiempirical. The data base employed for the fitting incorporates not only the present electronic structure calculations and those that we[12] and others[14−17] have previously reported, but also experimental information related to the equilibrium vibrational frequencies for the product conformations. Nevertheless, we suggest that the terminology is appropriate because the product vibrational frequencies could have easily been computed, and these topographical features of PES1 have virtually no effect upon the energy transfer and dissociation dynamics of vinyl bromide.

The minimum-energy structures for reactants and products are located using a damped trajectory method.[22] In this method, the atoms are initially placed in a configuration near the local minimum being sought. The kinetic energy of each atom is set to zero and Hamilton's equations of motion are integrated until the total kinetic energy attains a maximum. At this point, the integration is halted and all momenta are again set to zero. This procedure is repeated until the system potential energy converges to a local minimum. In all calculations, convergence to eight significant digits is obtained. For a 16-dimensional hypersurface, this damped trajectory method[22] is generally faster and more convenient to use than the usual steepest-descents/Newton−Raphson procedure because the energy is minimized with respect to all 15 independent coordinates simultaneously, and the necessary Hamiltonian equations of motion have already been programmed in preparation for the molecular dynamics computations to follow. The ΔE values with zero-point energy corrections included for the various reaction channels are listed in Table 6 where they are compared to the experimental and theoretical results. As can be seen, there is good agreement between the thermochemistry predicted by the analytic surfaces and that obtained from experiment and/or theory. The average absolute deviation between the two for the four reaction channels listed is 0.092 eV. The corresponding equilibrium geometries given by the analytic surfaces are compared with the experimental data in Table 7.

The calculated fundamental vibrational frequencies obtained from a normal-mode analysis using each of the three analytic potentials are given in Table 8 where they are compared to the

TABLE 6: Energies of Reaction with Zero-point Energy Corrections Included

	E (eV)		
reaction	analytic potential PES1	experiment or theory	reference
$C_2H_3Br \rightarrow C_2H_3 + Br$	2.973	3.101, 3.160	23,12
$C_2H_3Br \rightarrow H_2C{=}C + HBr$	3.012	2.922	24
$C_2H_3Br \rightarrow C{=}CHBr + H_2$	3.910	3.991	12
$H_2C{=}C \rightarrow HC{\equiv}CH$	−1.982	−1.990	15

TABLE 7: Comparison of Predicted Vinyl Bromide Equilbrium Geometries for Bond Lengths, Angles, and Dihedral Angles with Experiment[a]

variable	PES1	PES2	PES3	experiment[b]
		bond lengths		
C=C	1.3226	1.2928	1.2928	1.330
$C-H^3$	1.0706	1.0684	1.0684	1.077
C−Br	1.8943	1.8990	1.8990	1.890
$C-H^4$	1.0780	1.0771	1.0771	1.083
$C-H^5$	1.0710	1.0686	1.0686	1.085
		angles		
$C-C-H^3$	123.59	123.59	123.59	124.2
C−C−Br	123.76	123.76	123.76	122.5
$C-C-H^4$	119.52	119.54	119.54	118.7
$Br-C-H^3$	112.65	112.65	112.65	113.3
H^4-C-H^5	118.21	118.17	118.17	120.0
		dihedral angles		
$H^4-C-C-H^3$	0.0000	0.0000	0.0000	0.0000
$H^5-C-C-H^3$	180.0	180.0	180.0	180.0
$H^4-C-C-Br$	180.0	180.0	180.0	180.0
$H^5-C-C-Br$	0.0000	.0000	0.0000	0.0000

[a] Bond lengths are given in angstroms. Angles are given in degrees [b] Sverdlov, L. M.; Kovner, M. A.; Krainov, E. P. *Vibrational Spectra of Polyatomic Molecules*; Wiley: New York, 1974; pp 414−426.

measured IR and Raman experimental data. The table also compares the normalized normal-mode eigenvectors obtained from an ab initio SCF calculation using the same basis set as that employed in the MP4 calculations with those obtained using the analytic PES1 potential. The comparison is done in terms of the root mean-square deviations of the eigenvector components as defined in Table 8. As is generally the case, the stretching frequencies predicted by the MP4 calculations are too large by 5 to 10%. The bending frequencies given by the ab initio calculations are in better accord with experimental measurements, but they too are often too large. Because PES1 is fitted to these results, the frequencies obtained from this surface reflect these inaccuracies in the electronic structure results. The parameters in PES2 and PES3 have been adjusted to produce better agreement with the measured frequencies.

The potential barriers for the various reaction channels are obtained from the analytic surfaces using a combination of grid search and constrained, damped trajectory methods.[22,25] For HBr elimination, a two-dimensional search over C−Br and C−H distances is executed. Similarly for H_2 elimination, a search is executed over the two dissociating C−H bonds. At each node in the grid, a sequence of constrained, damped trajectory cycles are executed in which the virtual forces required to hold the two bond-distances of the grid fixed are incorporated. These damped trajectory cycles permit all atoms to relax to the most stable configuration associated with each grid point. The barrier heights are determined by iteration to the point at which all first derivatives of the potential are zero to three or more significant digits and a normal-mode analysis yields exactly one imaginary frequency.

TABLE 8: Comparison of Fundmental Vibrational Frequencies for Vinyl Bromide Obtained from the Analytic Surfaces with Experiment[a]

mode No.	description	RMS eigenvector deviations (Å)[b]	PES1	PES2	PES3	expt[c]
ν_1	C−C−Br bend	0.092	335	340	340	344
ν_2	CHBr wag	0.077	581	570	571	583
ν_3	C−Br stretch	0.025	593	603	603	613
ν_4	CH_2 wag	0.075	986	902	902	902
ν_5	CH_2−CHBr torsion	0.079	1053	953	953	942
ν_6	$C-C-H^5$ bend	0.104	1130	1022	1022	1006
ν_7	$C-C-H^3$ bend	0.079	1142	1231	1231	1256
ν_8	H−C−H bend	0.087	1375	1396	1396	1373
ν_9	C=C stretch	0.089	1765	1603	1603	1604
ν_{10}	C−H stretch	0.080	3386	3015	3008	3027
ν_{11}	C−H stretch	0.094	3478	3087	3085	3086
ν_{12}	C−H stretch	0.076	3520	3135	3136	3113

[a] The frequencies are reported in equivalent wave numbers (cm^{-1}). Eigenvector displacements are given in angstroms. [b] RMS Deviation $= (18)^{-1}\{\sum_{j=1}^{6}[(x^{ab} - x^{PES1})_j^2 + (y^{ab} - y^{PES1})_j^2 + (z^{ab} - z^{PES1})_j^2]\}^{1/2}$ where x^{ab} and x^{PES1} denote the x components of the normalized normal-mode displacement vectors obtained in the ab initio SCF calculations and those using the PES1 analytic surface, respectively, with analogous definitions for the y and z components. [c] Sverdlov, L. M.; Kovner, M. A.; Krainov, E. P. *Vibrational Spectra of Polyatomic Molecules*; Wiley: New York, 1974; pp 414−426. The experimental mode assignments are obtained by simple frequency matching.

For bromine-atom dissociation, the potential along the reaction coordinate on the analytic surfaces rises monotonically to that characteristic of the product state. There is no barrier to the back reaction. This is also the case for the MP4 calculations[12] where no transition state and no back-reaction barrier was found[12] for Br-atom dissociation. For three-center H_2 elimination, the MP4 calculations[12] predict a transition state and a small back-reaction barrier. In the case of three-center HBr elimination, the electronic structure calculations[12] indicate the presence of a transition state whose energy lies about 0.09 eV below the computed endothermicity for the reaction. Consequently, there is a potential well in the product valley for this dissociation channel but no back-reaction barrier. The analytic surfaces have no back-reaction barriers for the three-center dissociation processes. Table 9 compares the results.

Although the potential barriers for reaction are identical on all analytic surfaces, the reaction coordinate curvatures are not identical. The smaller equilibrium curvatures present on PES2 lead to curvatures along the three-center dissociation coordinates that are less than that for PES1. PES3 was formulated to reduce these curvatures even further. The reaction profiles for each surface for three-center HBr and H_2 elimination reactions are shown in Figure 7, parts A and B, respectively.

VI. Dissociation Dynamics of Vinyl Bromide

The dependence of the dissociation dynamics of vinyl bromide upon various topographical features of the potential-energy hypersurface have been investigated at several internal energies in the range 4.5−6.44 eV in excess of zero-point energy using classical trajectory methods.[25] Our conclusions are based upon a comparison of the computed dynamics on potential surfaces PES1, PES2, PES3, and EPS. Whenever possible, we also compare the results of these studies with the corresponding experimental data. The differences between PES1, PES2, and PES3 are described in Section IV. The methods employed to develop the EPS surface are much more empirical than is the case for PES1. The major differences are summarized in Table 10.

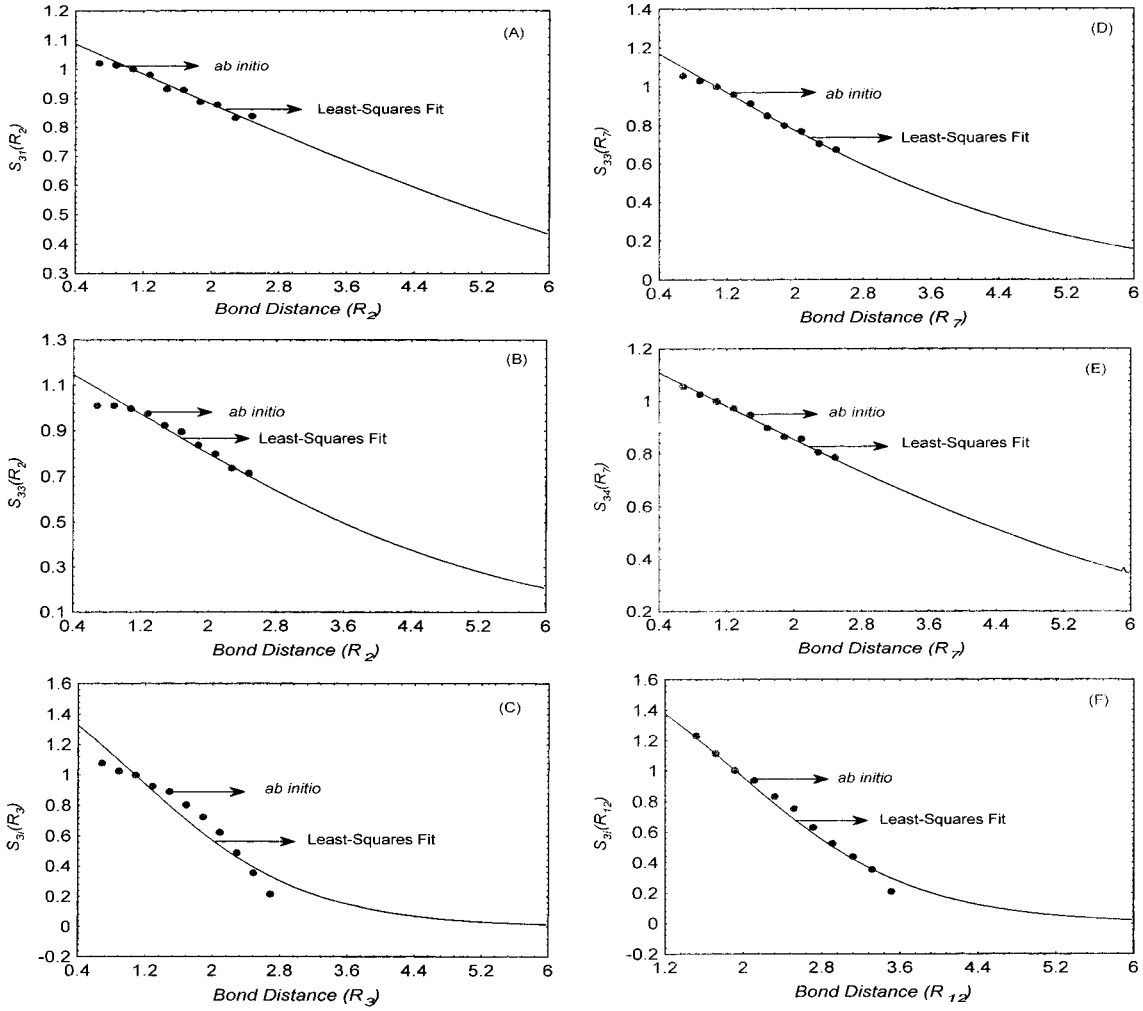

Figure 6. Comparisons of the functional dependence of $S_{3i}(R_v)$ upon R_v. The plotted points are the results obtained in the MP4 calculations using the procedures described in the text and eq 26 with $S_2(R_v)$ replaced with $S_{3i}(R_v)$. The curve is result of a least-squares fitting of eq 30 to the MP4 data. The fitted $S_{3i}(R_v)$ function is given in the figure. (A) $S_{31}(R_2)$, (B) $S_{33}(R_2)$, (C) $S_{31}(R_3)$, (D) $S_{33}(R_7)$, (E) $S_{34}(R_7)$, (F) $S_{34}(R_{12})$.

TABLE 9: Calculated Forward and Reverse Potential Barriers for Different Reaction Channels with Zero-Point Energy Corrections Included

	barriers (eV)				back reaction barriers (eV)			
reaction	PES1	PES2	PES3	MP4	PES1	PES2	PES3	MP4
$C_2H_3Br \rightarrow C_2H_3 + Br$	2.953	2.953	2.953	3.156[a]	0.000	0.000	0.000	0.000
$C_2H_3Br \rightarrow H_2C{=}C + HBr$	3.179	3.180	3.179	2.886[a]	0.000	0.000	0.000	0.000[a]
$H_2C{=}C \rightarrow HC{\equiv}CH$	0.017	0.017	0.017	< 0.088[b]	1.999	1.999	1.999	<2.078[b]
$C_2H_3Br \rightarrow C{=}CHBr + H_2$	4.198	4.198	4.198	4.322[a]	0.000	0.000	0.000	0.167[a]

[a] Reference 12. [b] References 14−17.

The initial states for the trajectories are prepared by insertion of zero-point energy into the vinyl bromide normal modes using projection methods.[22,26] Subsequently, Hamilton's equations of motion are integrated using a fourth-order Runge−Kutta procedure with a fixed step size of 2.038×10^{-16} s for a randomly chosen time period, t_p, given by

$$t_p = \xi\tau \tag{33}$$

where ξ is a random number chosen from a distribution that is uniform on the interval [0,1], and τ is the characteristic period of the lowest frequency vibrational mode in vinyl bromide. This procedure serves to randomize the vibrational phase angles for each trajectory. After completion of this integration, the desired excitation energy E is randomly partitioned among the twelve vibrational modes using projection techniques[22,26] with the initial rotational energy set to zero. With these initial states, trajectories are integrated until reaction occurs or until an upper limit of time, t_{max}, is exceeded. With this integration step size, energy is usually conserved to six significant digits. In some regions of the very complex vinyl bromide surface, the second derivatives of the potential become very large. Because we do not vary the step size, a few trajectories are lost because of failure to conserve energy. The fraction lost in this manner was 0.025. All calculations are executed using in-house programs.

Final states are determined using both distance and energy criteria. C−H or C−Br bond rupture is considered to have occurred whenever the bond distance exceeds 3.538 or 4.725 Å, respectively, and the relative translational energy of the products is greater than the residual C−H or C−Br attractive potential. The product phase space for three-center dissociation to HBr is defined to be those points for which $R_2 > 3.538$ Å

TABLE 10: Qualitative Comparison of the Methods Employed to Develop the ab Initio PES1 Potential Surface for Vinyl Bromide with Those Used in the Development of the Hybrid EPS Potential[12]

	method employed	
topological feature	PES1 surface	EPS surface[12]
	vinyl bromide	
equilibrium bond lengths	fit to ab initio data points	fit to experimental data
equilibrium angles	fit to ab initio data points	fit to experimental data
vibrational frequencies	fit to ab initio data points	fit to experimental data
bond stretching potentials	fit to ab initio data points	Morse potentials arbitrarily used
bending potentials	fit to ab initio data points	harmonic potentials forms used
dihedral potentials	fit to ab initio data points	arbitrary periodic form used. single parameter fitted to measured torsional frequency
bond energies	fit to ab initio data points	Morse parameters adjusted to give measured endo or exothermicities
stretch−bend coupling terms	fit to ab initio data points	arbitrary forms adjusted to yield the correct asymptotic limits.
dihedral-stretch coupling	fit to ab initio data points	arbitrary form adjusted to yield the correct asymptotic limits.
barrier heights	fit to ab initio data points	fit to ab initio data points
	decomposition products	
equilibrium bond lengths	fit to ab initio data points	fit to experimental data
equilibrium angles	fit to ab initio data points	fit to experimental data
vibrational frequencies	fit to experimental data	fit to experimental data
bond stretching potentials bending potentials dihedral potentials	functional forms same as for vinyl bromide with parameters fitted to experimental data.	functional forms same as for vinyl bromide with parameters fitted to experimental data.
bond energies	fit to experimental data	fit to experimental data
coupling terms	same as for vinyl bromide	same as for vinyl bromide

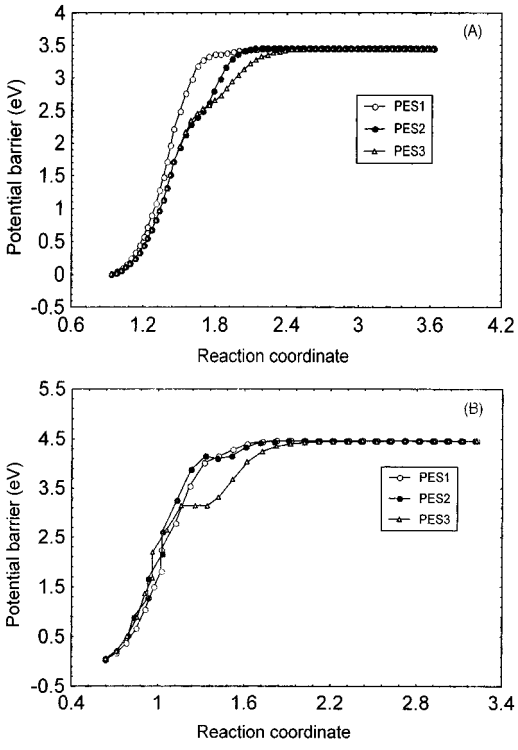

Figure 7. (A) Reaction profiles for three-center HBr elimination on PES1, PES2, and PES3. In each case, the reaction coordinate is taken as the distance between carbon atom 2 and the midpoint of the HBr distance. (B) Reaction profiles for three-center H_2 elimination on PES1, PES2, and PES3. In each case, the reaction coordinate is taken as the distance between carbon atom 1 and the midpoint of the H_2 distance.

and $R_{12} > 4.725$ Å combined with the requirement that the HBr internal vibrational−rotational energy lie below its dissociation limit. The product phase space for three-center dissociation to H_2 is defined to be those points for which $R_3 > 3.538$ Å and $R_7 > 3.538$ Å combined with the requirement that the H_2 internal vibrational−rotational energy lie below its dissociation limit.

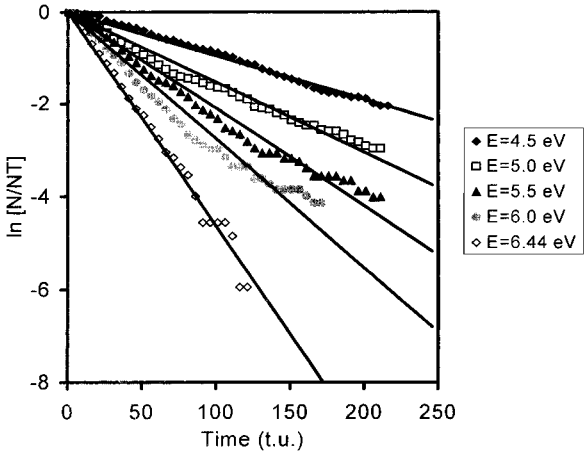

Figure 8. Logarithmic decay plots of $\ln[N/N_T]$ versus time at different excitation energies on potential surface PES1. N_T is the total number of trajectories computed, which is 400 in the above example, and N is the number of trajectories that have not reacted at time t. The points are the trajectory data. The lines are least-squares fits. The slopes of the lines yield the values of $k(E)$. Time is given in molecular time units (tu) where 1 tu = 0.010 19 ps.

If the internal energy exceeds these limits, dissociation to either 2H or H + Br is considered to have taken place.

The computed quantities of interest are first-order decay curves from which the microcanonical rate coefficients, $k(E)$, are obtained, the product branching ratios as a function of internal energy, the HBr vibrational energy distribution and the dissociation mechanisms.

A. Total Decomposition Rates. The total decomposition rates of vinyl bromide on PES1, PES2, and PES3 have been obtained at each internal energy investigated by least-squares fitting of the computed decay plots. Figure 8 shows the results obtained on PES1 for $E = 4.5$, 5.0, 5.5, 6.0, and 6.44 eV. The points are the trajectory results obtained from a total of 400 trajectories with $t_{max} = 250$ tu (1 tu = 0.010 19 ps). The lines shown in the plot are the least-squares fits to the data. The negative slope of

TABLE 11: Comparison of the Total Decomposition Rate Coefficients of Vinyl Bromide at Different Internal Energies on PES1, PES2, and PES3[a]

	rate coefficients, k(E) (ps^{-1})			
energy (eV)	PES1	PES2	PES3	EPS
4.50	0.932 ($\pm 9.9 \times 10^{-5}$)	0.893 ($\pm 6.3 \times 10^{-5}$)	0.736 ($\pm 4.8 \times 10^{-5}$)	0.350
5.00	1.492 ($\pm 2.2 \times 10^{-4}$)	1.551 ($\pm 1.4 \times 10^{-4}$)	1.354 ($\pm 1.8 \times 10^{-4}$)	0.540
5.50	2.061 ($\pm 3.4 \times 10^{-4}$)	3.013 ($\pm 3.0 \times 10^{-4}$)	2.208 ($\pm 3.4 \times 10^{-4}$)	1.040
6.00	2.709 ($\pm 6.4 \times 10^{-4}$)	3.984 ($\pm 8.4 \times 10^{-4}$)	3.445 ($\pm 6.6 \times 10^{-4}$)	1.490
6.44	4.553 ($\pm 7.6 \times 10^{-4}$)	4.652 ($\pm 1.2 \times 10^{-3}$)	4.995 ($\pm 5.8 \times 10^{-4}$)	2.110

[a] The results previously reported by Abrash et al.[12] using a predominately empirical potential surface are given in the column labeled EPS. The uncertainties in the slopes of the least-square fits are given within the parentheses

TABLE 12: Ratio of k_s(E) for Potential Surface s to that for PES1 as a Function of Excitation Energy

	$\frac{k_s(E)}{k_{PES1}(E)}$		
energy (eV)	surface s: PES2	PES3	EPS
4.5	0.958	0.790	0.376
5.0	1.039	0.908	0.362
5.5	1.462	1.071	0.505
6.0	1.471	1.272	0.550
6.44	1.022	1.097	0.463

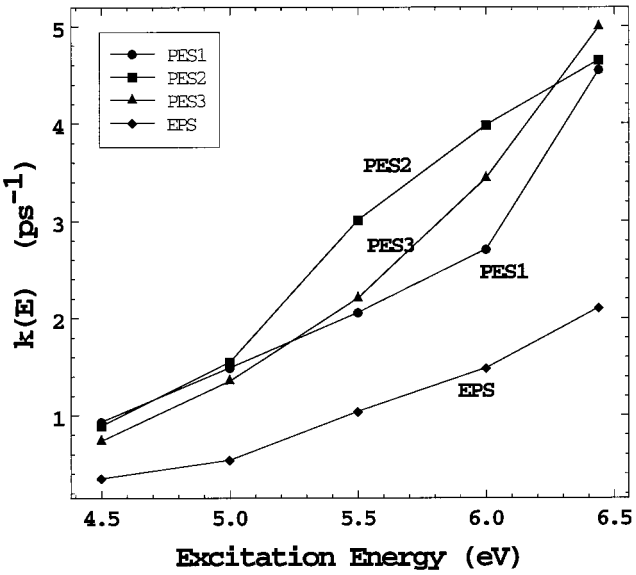

Figure 9. Total decomposition rate coefficients as a function of internal excitation energy on the four potential surfaces. The computed results are shown as points connected by straight-line segments to enhance the visual clarity.

these lines give the corresponding value of $k(E)$. The near linearity of the decay curves show that the total dissociation is well described by a first-order rate law. The results obtained on surfaces PES2, PES3, and EPS[12] are qualitatively similar to those shown in Figure 8.

The rate coefficients for all surfaces are tabulated in Table 11. The table also presents the results previously obtained by Abrash et al.[12] using the EPS surface. The uncertainties in the slopes are given inside the parentheses. The ratios of $k_s(E)/k_{PES1}(E)$ for surface s are listed in Table 12 for PES2, PES3, and EPS as a function of the excitation energy. A plot of the results on all potential surfaces is shown in Figure 9. It is clear that close fitting of the potential surface curvatures near equilibrium to the measured fundamental vibrational frequencies makes very little difference in the computed total decomposition rate coefficients. Most of the ratios are near unity with the maximum variation being 47%. The same conclusion can be drawn about the effect of the reaction coordinate curvatures because the rate coefficients on PES2 and PES3 are nearly the same. The maximum difference is 37%. The average absolute percent difference is 19%. There is, however, a significant difference between the decomposition rates obtained on the more empirical EPS surface and those obtained on the *ab initio* potential. The decomposition rates computed on the EPS surface are between a factor of 2 to 3 less than the corresponding values on PES1. At present, there are no experimental data available for the total decomposition rates of vinyl bromide as a function of internal excitation energy.

TABLE 13: Percentage Yields of Products on PES1, PES2, PES3, and EPS Surfaces[a]

potential	excitation	percentage yield of product			
surface	energy (eV)	HBr	H_2	Br	H
PES1	4.5	81 ($\pm$2)	0	1 ($\pm$44)	4 ($\pm$23)
	5.0	89 ($\pm$2)	0.5 ($\pm$70)	3 ($\pm$31)	3 ($\pm$31)
	5.5	87 ($\pm$2)	5 ($\pm$22)	3 ($\pm$31)	3 ($\pm$27)
	6.0	86 ($\pm$2)	8 ($\pm$17)	2 ($\pm$40)	3 ($\pm$28)
	6.44	85 ($\pm$2)	7 ($\pm$19)	3 ($\pm$30)	5 ($\pm$23)
PES2	4.5	72 ($\pm$3)	0	2 ($\pm$37)	11 ($\pm$14)
	5.0	84 ($\pm$2)	0	2 ($\pm$38)	10 ($\pm$15)
	5.5	85 ($\pm$2)	1 ($\pm$44)	5 ($\pm$22)	9 ($\pm$16)
	6.0	90 ($\pm$2)	1 ($\pm$50)	4 ($\pm$25)	5 ($\pm$21)
	6.44	88 ($\pm$2)	1 ($\pm$57)	6 ($\pm$21)	5 ($\pm$23)
PES3	4.5	73 ($\pm$3)	0.5 ($\pm$70)	4 ($\pm$24)	2 ($\pm$33)
	5.0	86 ($\pm$2)	1 ($\pm$50)	5 ($\pm$22)	3 ($\pm$30)
	5.5	89 ($\pm$2)	2 ($\pm$40)	7 ($\pm$19)	2 ($\pm$38)
	6.0	91 ($\pm$2)	3 ($\pm$31)	4 ($\pm$24)	2 ($\pm$37)
	6.44	86 ($\pm$2)	3 ($\pm$31)	11 ($\pm$14)	0.3 ($\pm$99)
EPS	4.5	88	2	11	0
	5.0	89	4	8	0
	5.5	74	16	9	1
	6.0	63	29	7	2
	6.44	44	48	5	3

[a] The total percent yields for all products do not sum to 100% because some trajectories do not react at times less than t_{max}. The percent statistical uncertainties are given within the parentheses.

B. Branching Ratios. The product branching percentages for various reaction channels in the decomposition of vinyl bromide have been computed on PES1, PES2, and PES3. These results are given in Table 13 where they are compared with data previously reported by Abrash et al.[12] using the EPS empirical potential. The statistical uncertainties are given inside the parentheses. These uncertainties, Δ, are computed from[25]

$$\Delta = 100\left[\frac{N - N_R}{NN_R}\right]^{1/2} \tag{34}$$

where N is the total number of trajectories computed, and N_R is the total number that reacted to produce a given product. Comparison of the results obtained with the ab initio surface PES1 and the two derivative surfaces, PES2 and PES3, reveals that only minor differences exist. On all surfaces, the major decomposition product at all energies investigated is HBr. The variations in the percentage yields of the minor products, in

many cases, fall within the combined statistical uncertainties of the calculations. Exceptions include hydrogen and bromine-atom dissociation reactions on PES2 and PES3. When the C−H vibrational frequencies are adjusted to more nearly match the spectroscopic data on PES2, there is a significant enhancement of the hydrogen-atom dissociation probability. The only effect of the reaction coordinate curvature variations introduced in PES3 is some enhancement of bromine-atom dissociation at the highest energy.

In contrast, there are major differences in the branching ratios computed on PES1 and the empirical EPS surface. On the EPS surface, three-center H_2 dissociation competes equally with three-center HBr dissociation at 6.44 eV. As the internal energy rises, the H_2 dissociation channel monotonically increases in importance, whereas that for HBr dissociation declines steadily. The origin of these differences may lie in the significant variations of the topology of PES1 and EPS that arise because of the very different formulation procedures used in the development of the potentials. These procedures are summarized in Table 10. This view suggests that the problem lies primarily in the EPS surface. It leads to the conclusion that although some dynamic features of a complex reaction, such as total decomposition rate, may be reasonably modeled using predominately empirical surfaces, other features, such as branching ratios, may be in serious error. There is, however, a second possibility. The PES1, PES2, and PES3 potentials do not include the four-center dissociation channels leading to HBr and H_2 elimination, whereas the EPS surface does. Although our previous calculations[12] have shown that such four-center dissociation rarely occurs, the possibility exists that at higher internal energies, the system might explore regions of phase space that correspond to stretching of the bonds involved in a four-center reaction even though such a process does not proceed to completion. If this is the case, then the problem may lie with the ab initio potential that does not include the four-center dissociation channels.

There are no experimental measurements of branching ratios for vinyl bromide decomposition that have been reported. The present findings as well as those reported by Abrash et al.[12] are in accord with the theoretical studies of the dissociation mechanisms for ethylene and vinyl chloride reported by Jensen et al.[3] and Riehl and Morokuma,[6] respectively. In both cases, H_2 and HCl dissociation was predicted to occur via a three-center process. These predictions are in agreement with the experimental observations published by Okabe and McNesby[4] and by Balko et al.,[5] Ausloss et al.,[7] Reiser et al.[8], and Huang et al.[9] Similar measurements are needed for the vinyl bromide system.

It should be noted that the although Br-atom dissociation has the lowest potential barrier of any of the decomposition channels on PES1, PES2, and PES3, it plays a relatively minor role in the overall decomposition process. This emphasizes the danger inherent in utilizing energies of stationary points and transition states alone to predict reaction mechanism when the available energy is significantly in excess of the potential barriers. Such a procedure ignores the importance of dynamic effects. In this case, there is a large energy-transfer bottleneck in moving internal energy into the C−Br stretching coordinate because of the large bromine-atom mass. This bottleneck greatly reduces the frequency of bromine-atom dissociation.

C. HBr Internal Energy Distributions. To assess the importance of equilibrium and reaction coordinate curvature upon the energy partitioning dynamics in the dissociation process, we have computed the product HBr internal vibrational energy distributions. This determination also permits us to execute a direct comparison with measured results for this distribution. Recently, Dai et al.[27] have carried out photolysis experiments on vinyl bromide at 193 nm (6.44 eV). The IR emission from vibrationally excited HBr is measured and the pristine vibrational-state distribution determined. They find that their results are essentially Boltzmann with an effective temperature of $T_{vib}^{expt.} = 6999$ K.

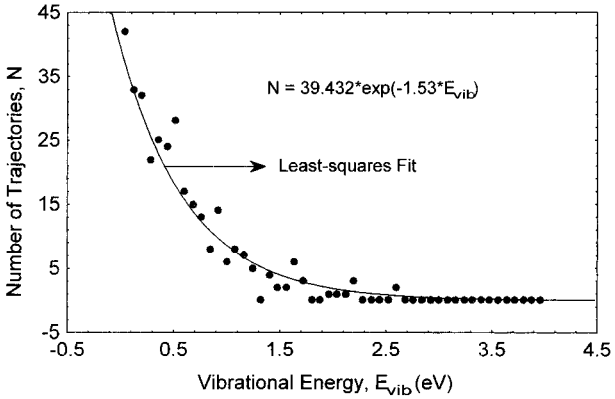

Figure 10. Computed classical distribution of HBr vibrational energies on PES1 after HBr elimination from vinyl bromide at an excitation energy of 6.44 eV. The curve is a least-squares fit of a Boltzmann distribution to the trajectory data which are given by the points.

Because we know the momentum components of all atoms at each moment of time from the trajectory results, it is a simple matter to project out the component of H−Br relative velocity associated with vibrational motion, v_{vib}^{HBr}. The total HBr vibrational energy is then given by

$$E_{vib}^{HBr} = 0.5\,\mu_{HBr}\,[v_{vib}^{HBr}]^2 + V_{HBr} + D \qquad (35)$$

where μ_{HBr} is the HBr reduced mass, V_{HBr} is the HBr interatomic potential, which is assumed to be a Morse potential in the present calculations, and D is the HBr potential well depth.

The distribution of HBr vibrational energies is obtained from the results of all trajectories resulting in three-center HBr dissociation. For each trajectory, eq 35 is used to compute E_{vib}^{HBr}. The energy range from zero to 4.0 eV is then divided into 50 equally spaced bins, and the results for E_{vib}^{HBr} are used to determine the number of trajectories resulting in HBr vibrational energies that lie within the energy range characteristic of each bin. A plot of these data yields the classical HBr vibrational energy distribution. The result for surface PES1 at an excitation energy of 6.44 eV is shown in Figure 10. Inspection of the plot shows the distribution to be noninverted and near-Boltzmann in character. Consequently, we may fit the results to the Boltzmann distribution law

$$N(E_{vib}^{HBr}) = A \exp\left[-\frac{E_{vib}^{HBr}}{kT}\right] \qquad (36)$$

where $N(E_{vib}^{HBr})$ is the number of trajectories in the energy bin whose energy midpoint is E_{vib}^{HBr}. The solid curve shown in Figure 10 is a plot of $N(E_{vib}^{HBr})$ versus E_{vib}^{HBr} with $A = 39.432$ and $(kT)^{-1} = 1.53$.

To provide a direct quantitative comparison with the experimental results obtained by Dai et al.,[27] we quantize the final HBr vibrational distribution as follows: The energy of the vth HBr vibrational state can be written as

$$E_v^{HBr} = (v + 0.5)\,h\nu_o - (v + 0.5)^2\omega_e x_e \qquad (37)$$

TABLE 14: Comparisons of Normalized Relative HBr Vibration-state Distributions Obtained from Trajectory Calculations on PES1, PES2, PES3, and from the Photolysis experiments[27] at an Excitation Energy of 6.44 EV (193 nm)

	normalized distributions			
HBr vibration state	PES1	PES2	PES3	expt[a]
1	0.406	0.406	0.403	0.409
2	0.246	0.246	0.246	0.247
3	0.161	0.160	0.161	0.151
4	0.087	0.087	0.088	0.084
5	0.061	0.061	0.062	0.060
6	0.039	0.039	0.040	0.039

[a] Reference 27.

where ν_o is the measured fundamental HBr frequency and $\omega_e x_e$ is the measured aharmonicity factor. The values of these parameters are taken from Herzberg.[28] In order for HBr to be in the υth vibrational state, its vibrational energy must be at least equal to E_υ^{HBr}. Therefore, we assume that HBr will be in the v*th* vibrational state if its vibrational energy lies in the range $E_{vib}^{HBr} \leq E_{vib}^{HBr} < E_{\upsilon+1}^{HBr}$. With this assumption, the number of HBr molecules in vibrational state υ, N_υ, is given by

$$N_\upsilon = \int_{E_\upsilon^{HBr}}^{E_{\upsilon+1}^{HBr}} A \exp\left[-\frac{E_{vib}^{HBr}}{kT}\right] dE_{vib}^{HBr} \qquad (38)$$

When the calculations are done on surface PES1, eq 38 becomes

$$N_\upsilon = 39.432 \int_{E_\upsilon^{HBr}}^{E_{\upsilon+1}^{HBr}} \exp[-1.53\, E_{vib}^{HBr}]\, dE_{vib}^{HBr} = 25.773\, [\exp\{-1.53\, E_\upsilon^{HBr}\} - \exp\{-1.53\, E_{\upsilon+1}^{HBr}\}] \qquad (39)$$

where E_υ^{HBr} and $E_{\upsilon+1}^{HBr}$ are given by eq 37.

The experiments carried out by Dai et al.[27] do not permit the concentration of HBr in the ground vibrational state to be determined because there is no IR emission from the $\upsilon = 0$ vibrational state. Therefore, direct comparison of theory with experiment requires that we normalize both the experimental and computed excited-state vibrational distributions to a common constant. This is done by requiring that $\sum_{\upsilon=1}^{\infty} N_\upsilon = 1$. Table 14 presents the relative HBr vibrational state populations obtained from PES1, PES2, and PES3 and from the experiments.[27]

To obtain an effective temperature from our computed data, we have fitted the results given in Table 14 to a quantized Boltzmann distribution function

$$P(E_\upsilon^{HBr}) = A \exp\left[-\frac{(\upsilon + 0.5)\, h\nu_o - (\upsilon + 0.5)^2 \omega_e x_e}{kT}\right] \qquad (40)$$

using least-squares methods with A and T being adjustable parameters. In eq 40, the $P(E_\upsilon^{HBr})$ values are the normalized relative populations given in Table 14. The resulting vibrational temperatures are 7084, 7075, and 7165 K for PES1, PES2, and PES3, respectively. Figure 11 shows a comparison between the ab initio results on PES1 and experiment along with the fit produced by eq 40 with a vibrational temperature of 7084 K.

The virtually exact agreement between the HBr vibrational distributions obtained on PES1, PES2, and PES3 shown in Table 14 and Figure 11 indicates that energy partitioning between HBr and vinylidene in three-center HBr dissociations is nearly independent of the potential-energy curvatures at equilibrium and along the reaction coordinate. The near exact agreement between the theoretical and the experimental distributions

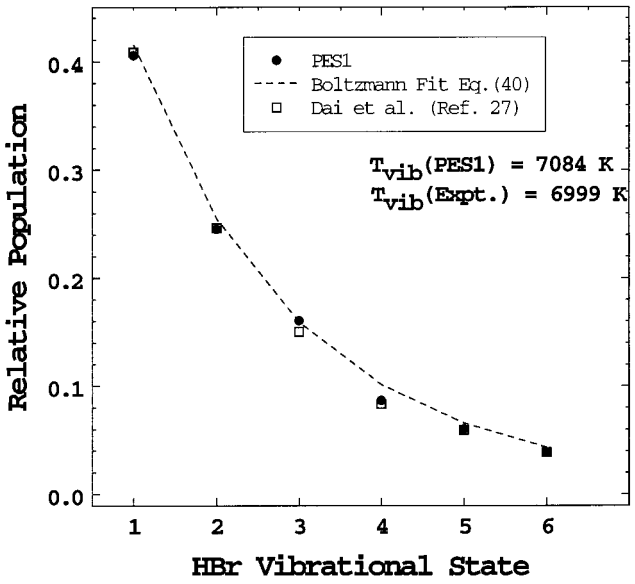

Figure 11. Comparison between HBr vibrational-state energy distributions after HBr elimination from vinyl bromide at 6.44 eV excitation energy. The dashed curve is a fit to a Boltzmann distribution with a vibrational temperature of 7084 K. (●) computed data from PES1 surface (□) Experimental data, Reference 27.

suggests that the important topographical features of the potential surface that do exert major influence upon this energy partitioning are correctly described by the fitting to the ab initio calculations. Furthermore, this near exact agreement provides compelling evidence of the correctness of our previously drawn conclusion[12] that HBr dissociation occurs on the electronic ground-state potential surface after internal conversion from the excited state produced by the 193 nm photolysis.

D. Ground-State Dissociation Mechanisms. By monitoring the temporal behavior of appropriate geometric variables, it is a simple matter to determine the mechanism or mechanisms for three-center dissociations of HBr and H_2. The results obtained using PES1, PES2, and PES3 are qualitatively identical. This again demonstrates that as long as the potential surface is fitted to extensive, high-level ab initio calculations, small variations in the potential curvatures do not produce major changes in the observed dynamics.

We observe three different mechanisms for HBr elimination reactions but only one for H_2 dissociation. The three dissociation modes for HBr production are illustrated in Figure 12, parts A, B, and C, where the temporal behavior of the C−Br, C−H[3], and the H[3]−Br interatomic distances is shown for typical reactions involving each of the three dissociation mechanisms. These interatomic distances are R_{12}, R_2, and R_{13}, respectively, in the notation illustrated in Figure 1. The trajectory whose details are shown in Figure 12A is typical of those in which HBr dissociation involves a simultaneous cleavage of both the C−H and C−Br bonds. In the case shown, this concerted bond rupture occurs around 57 t.u. into the trajectory. After bond scission, a slow, oscillatory motion of the C−H distance is observed. This oscillation is due to HBr rotation. Because of the asymmetric transition state,[12] rotational energy is expected to be imparted to HBr being formed in a concerted dissociation process.

Figure 12B illustrates HBr dissociation via a mechanism that involves C−H bond rupture followed by transfer of the hydrogen atom to the bromine atom. This intermediate lives for a short period after which the process is either reversed to reform vinyl bromide or the C−Br bond ruptures to form HBr and vinylidene.

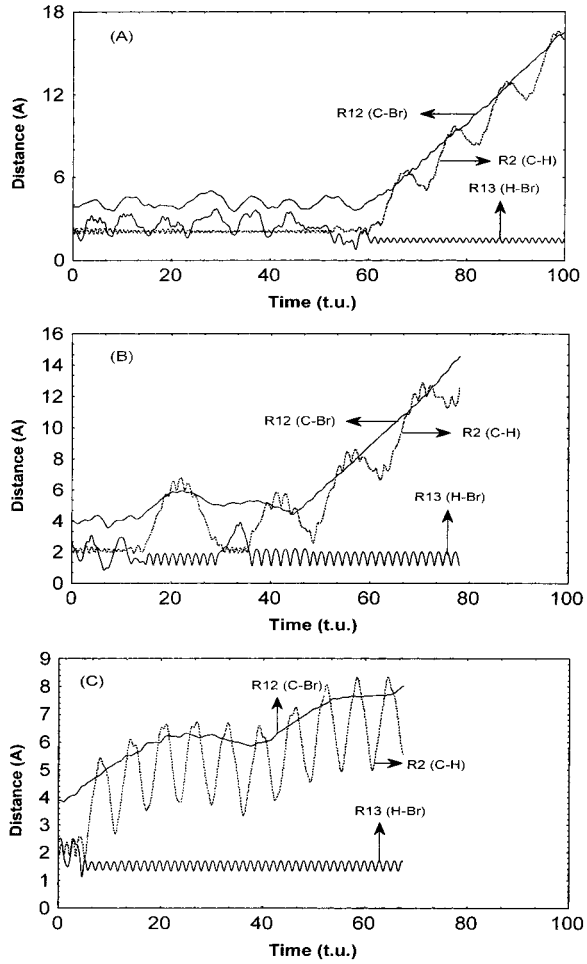

Figure 12. Mechanistic details for three-center HBr elimination reactions. The plot shows the temporal variations of the C−Br distance (R_{12}), the C−H[3] distance (R_2) and the H[3]−Br distance (R_{13}). Time is given in units of 0.010 19 ps. The curves for R_{12} and R_2 are displaced upward by 1 Å to enhance the visual clarity of the plot. (A) concerted dissociation mechanism, (B) sequential mechanism involving hydrogen-atom transfer followed by C−Br bond scission, (C) concerted dissociation with subsequent formation of a van der Waals complex.

For the trajectory illustrated in Figure 12B, the initial C−H bond rupture occurs around 13 t.u. Simultaneously, the H−Br distance decreases to a value characteristic of the H−Br equilibrium distance. Clearly, H[3] has transferred to the bromine atom which is still partially bonded to the carbon atom. Examination of the C−Br distance after the H-atom transfer shows the bond to have extended. Around 25 t.u., the transfer is seen to reverse momentarily reforming vinyl bromide. At 37 t.u., we again see hydrogen-atom transfer to the bromine atom. This time, the C−Br bond breaks around 47 t.u. before the transfer process can be reversed the HBr and vinylidene products are formed. Again, we see the presence of rotational energy in the newly formed HBr. This type of transfer mechanism is not unexpected. In 1978−1980, Holmes and Setser[29] suggested that four-center hydrohalogen elimination reactions would proceed by migration of a hydrogen atom to the halogen followed by rupture of the C-halogen bond. Previous theoretical studies[10j,22] of the gas-phase decomposition of 1,2-difluoroethane-d_4 explicitly confirmed the suggestion made by Holmes and Setser.[29] The present results demonstrate that three-center dissociations can also involve such a transfer mechanism.

A third mechanism for HBr dissociation involves a concerted C−H and C−Br bond rupture followed by the formation of a short-lived van der Waals complex. Figure 12C shows the details for one such reaction. Around 5 t.u., concerted C−Br and C−H bond scission occurs. However, the newly formed HBr molecule remains in the near vicinity of vinylidene for about 40 t.u., after which it slowly moves away.

The only dissociation mechanism we have observed for three-center H_2 elimination involves concerted bond rupture of both C−H bonds. The trajectory details are qualitatively similar to those seen in Figure 12A.

Abrash et al.[12] observed only one dissociation mechanism for three-center HBr elimination when the primarily empirical EPS surface was used in the calculations. This is in marked contrast to the three dissociation processes seen in the present calculations. Therefore, it appears that while some features of the dynamics are very similar on both empirical and ab initio surfaces, others exhibit significant differences. The total decomposition rates as a function of internal excitation energy, the branching ratios at lower excitation energies, and the H_2 dissociation mechanism are examples of dynamic features that are described with fair accuracy by the empirical surface. The branching ratios at higher energies and the HBr dissociation mechanisms are dynamic features whose characteristics are markedly different on the empirical and ab initio surfaces. As noted previously, this might be due to topological features of the EPS potential that are poor representations of the experimental surface. Alternatively, the differences might be the result of our having eliminated consideration of the four-center dissociation channels in the development of the ab initio surfaces.

VII. Summary

The reaction dynamics of vibrationally excited vinyl bromide have been investigated using classical trajectory methods on a global, analytic potential-energy hypersurface (PES1) that is developed primarily by least-squares fitting of appropriately chosen functional forms to the results of ab initio electronic structure calculations. These calculations are carried out at the MP4 level of theory with all single, double, and triple excitations included. A 6-31G(d,p) basis set is employed for the carbon and hydrogen atoms. Huzinaga's[19] (4333/433/4) basis set augmented with split outer s and p orbitals (43321/4321/4) and a polarization f orbital with an exponent of 0.5 is used for the bromine atom. A second potential surface (PES2) is developed by empirical adjustment of the surface curvatures at equilibrium so as to produce good agreement between the vinyl bromide vibrational frequencies obtained spectroscopically and those predicted by the surface. In the execution of this fitting, the surface parameters are adjusted so as to maintain the other topographical features of the surface as constant as possible. The curvatures along the three-center elimination reaction coordinates for PES2 are then arbitrarily varied to produce a third surface (PES3). Again, to the extent possible, the surface parameters are varied to a avoid altering the remaining features of the potential. The dissociation dynamics of vinyl bromide on each of these surfaces are computed using classical trajectory methods and the results compared with each other and with previously reported data obtained using a much more empirical potential surface (EPS). These comparisons show the following:

(1) Total decomposition rates are well described by first-order kinetics. The microcanonical rate coefficients are obtained from the slopes of computed decay curves. Only small differences between the results on PES1, PES2, and PES3 are observed. Consequently, potential-surface curvature variations do not produce significant changes in the dissociation rates. There are significant quantitative differences between the rates on the

empirical EPS surface and those obtained for the ab initio potential. These differences are a factor of two to three depending upon the excitation energy. However, the results obtained with the EPS potential show no major qualitative differences from the PES1 rates.

(2) There are some minor quantitative differences in the computed branching ratios on PES1, PES2, and PES3. In some cases, the differences are less than the combined error limits. At low excitation energies, the results on PES1 are in fair accord with those obtained using the EPS potential. However, at the highest energy investigated (6.44 eV), there are major qualitative differences present. The branching ratios obtained with empirical surface are not even in qualitative accord with those predicted by the ab initio surface. These differences might be the result of numerous topographical features of the EPS potential being very poor representations of the experimental surface. Alternatively, they might be due to the fact that the four-center elimination channels, which are included in the EPS formulation, have not been considered in our development of the ab initio surfaces.

(3) The vibrational state energy distribution of HBr molecules formed via three-center elimination reactions is Boltzmann with a characteristic temperature of 7084 K. These results are in near exact agreement with the experimentally determined distribution.[27] The distributions obtained on PES1, PES2, and PES3 are essentially identical. This evidence suggests that the ab initio surface is an accurate representation of the experimental potential and that three-center HBr elimination occurs on the ground-state surface after internal conversion from the excited state formed in the 193 nm photolysis.[27]

(4) Three dissociation mechanisms for HBr elimination are found on the PES1, PES2, and PES3 potentials, whereas only one is found when the EPS surface is employed. The possible reasons for this difference are those discussed under point 2.

On the basis of the above evidence, we conclude that although useful information related to polyatomic reaction dynamics can be obtained by employing empirical surfaces, it is necessary to exercise great care when proceeding in this fashion. It is possible that the results may not even be qualitatively correct. We also conclude that small variations in the potential surface curvatures at equilibrium and along the reaction coordinates do not exert major influence upon the dissociation dynamics.

Acknowledgment. We thank Professor Dean-Kuo Liu et al.[27] for providing their experimental results, prior to publication, on the initial HBr vibrational-energy distribution obtained upon unimolecular decomposition of vinyl bromide after photolysis at 193 nm.

Supporting Information Available: The results of the electronic structure calculations for all nuclear conformations considered (299 total conformations) in this investigation are given in tabular form. The tables include the total relaxed MP4 energies in hartrees and the scaled energies in eV as a function of the interatomic distances between bonded atoms, the three C−C−H angles, the C−C−Br angle, and the torsional angle. Several tables are also available in which the effect of coordinate couplings upon the potential are evaluated. This material is available free of charge via the Internet at http://pubs.acs.org.

References and Notes

(1) See, for example: Liu, B. *J. Chem Phys.* **1973**, *58*, 1925. Siegbahm, P.; Liu, B. *J. Chem Phys.* **1978**, *68*, 2457. Liu, B. *J. Chem Phys.* **1984**, *80*, 581.

(2) See, for example: (a) Bakkas, N.; Bouteiller, Y.; Loutellier, A.; Perchard, J. P.; Racine, S. *J. Chem. Phys.* **1993**, *99*, 3335. (b) Wladlowski, B. D.; East, A. L. L.; Mihalick, J. E.; Allen, W. D.; Brauman, J. I. *J. Chem. Phys*. **1994**, *100*, 2058. (c) Walch, S. P. *J. Chem. Phys*. **1993**, *98*, 3163. (d) Walch, S. P. *J. Chem. Phys*. **1993**, *99*, 5295. (e) Robertson, S. H.; Wardlaw, D. M.; Hirst, D. M. *J. Chem. Phys*. **1993**, *99*, 7748. (f) Mebel, A. M.; Morokuma, K.; Lin, M. C. *J. Chem. Phys*. **1994**, *101*, 3916. (g) Maluendes, S. A.; McLean, A. D.; Yamashita, K.; Herbst, E. *J. Chem. Phys*. **1993**, *99*, 2812.

(3) Jensen, J. H.; Morokuma, K.; Gordon, M. S. *J. Chem. Phys*. **1994**, *100*, 1981.

(4) Okabe, H.; McNesby, J. R. *J. Chem. Phys*. **1962**, *36*, 601.

(5) Balko, B. A.; Zhang, J.; Lee, Y. T. *J. Chem. Phys*. **1992**, *97*, 935.

(6) Riehl, J. F.; Morokuma, K. *J. Chem. Phys*. **1994**, *100*, 8976.

(7) Ausloos, P.; Rebbert, R. E.; Wijnen, M. H. *J. Res. Nat. Bur. Std*. **1973**, *77A*, 243.

(8) Reiser, C.; Lussier, F. M.; Jensen, C. C.; Steinfeld, J. I. *J. Am. Chem. Soc*. **1979**, *101*, 350.

(9) Huang, Y.; Yang, Y.; He, G.; Gordon, R. J. *J. Chem. Phys*. **1993**, *99*, 2752.

(10) See, for example: (a) Sewell, T. D.; Thompson, D. L. *J. Chem. Phys*. **1990**, *93*, 4077. (b) Marks, A. J. *J. Chem. Phys*. **1994**, *100*, 8096. (c) Rice, B. M.; Thompson, D. L. *J. Chem. Phys.* **1990**, *93*, 7986. (d) Alimi, R. V.; Apkarian, V. A.; Gerber, R. B. **1993**, *98*, 331. (e) Lendvay G.; Schatz, G. C. *J. Chem. Phys*. **1992**, *96*, 4356. (f) Lendvay G.; Schatz, G. C. *J. Chem. Phys*. **1993**, *98*, 1034. (g) Budenholzer, F. E.; Chang, M. Y.; Huang, K. C. *J. Phys. Chem*. **1994**, *98*, 12501. (h) Raff, L. M. *J. Chem. Phys*. **1990**, *93*, 3160. Raff, L. M. *J. Chem. Phys*. **1992**, *97*, 7459. (i) Raff, L. M. *J. Phys. Chem.* **1987**, *91*, 3266. Raff, L. M. *J. Phys. Chem*. **1988**, *92*, 141. (j) Raff, L. M.; Graham, R. W. *J. Phys. Chem*. **1988**, *92*, 5111.

(11) For examples of this approach to the development of potential surfaces, see: (a) Cho, Y. J.; Vande Linde, S. R.; Zhu, L.; Hase, W. L. *J. Chem. Phys*. **1992**, *96*, 8275. (b) Vande Linde, S. R.; Hase, W. L. *J. Phys. Chem*. **1990**, *94*, 6148 and *J. Chem. Phys.* **1990**, *93*, 7962. (c) Hase, W. L.; Cho, Y. J. *J. Chem. Phys*. **1993**, *98*, 8626. (d) Jordan, M. J. T.; Gilbert, R. G. *J. Chem. Phys.* **1995**, *102*, 5669. (e) Joseph, T. R.; Steckler, R.; Truhlar, D. G. *J. Chem. Phys*. **1987**, *87*, 7036. (f) Klippenstein, S. J.; Radivoyevitch, T. *J. Chem. Phys*. **1993**, *99*, 3644. (g) Hase, W. L.; Darling, C. L.; Zhu, L. *J. Chem. Phys*. **1992**, *96*, 8295. (h) Hu, X.; Hase, W. L. *J. Chem. Phys*. **1991**, *95*, 8073; *ibid*, "**Erratum Note**" **1992**, *96*, 5558. (i) Truong, T. N.; Truhlar, D. G. *J. Chem. Phys*. **1990**, *93*, 1761. Truong, T. N.; Truhlar, D. G. *J. Chem. Phys*. "**Erratum Note**" **1992**, *97*, 8820. (j) Agrawal, P. M.; Thompson, D. L.; Raff, L. M. *J. Chem. Phys*. **1990**, *92*, 1069. (k) Sorescu, D. C.; Thompson, D. L.; Raff, L. M. *J. Chem. Phys*. **1994**, *101*, 3729; Sorescu, D. C.; Thompson, D. L.; Raff, L. M. *J. Chem. Phys*. **1995**, *102*, 7910.

(12) Abrash, S. A.; Zehner, R. W.; Mains, G. J.; Raff, L. M. *J. Phys. Chem*. **1995**, *99*, 2959.

(13) Huzinaga, S. *J. Chem. Phys.* **1965**, *42*, 1293.

(14) Osamura, Y.; Schaefer III, H. F.; Gray, S. K.; Miller, W. H. *J. Am. Chem. Soc*. **1981**, *103*, 1904.

(15) Krishnan, R.; Frisch, M. J.; Pople, J. A.; Von R. Schleyer, P. *Chem. Phys. Lett.* **1981**, *79*, 408.

(16) Smith, B. J.; Smernik, R.; Radom, L. *Chem. Phys. Lett.* **1992**, *188*, 589.

(17) Halvick, Ph.; Liotard, D.; Rayez, J. C. *Chem. Phys*. **1993**, *177*, 69.

(18) *Gaussian 94*, Revision E.2; Gaussian, Inc. Pittsburgh, PA, 1995.

(19) Huzinaga, S.; Andzelm, J.; Klobukowski, M.; Radzio-Andzelm, E.; Sakai, Y.; Tatewaki, H. *Gaussian Basis Sets for Molecular Calculations*; Elsevier: Amsterdam, 1984.

(20) Dasgupta, S.; Goddard, W. A., III. *J. Chem. Phys*. **1989**, *90*, 7207.

(21) Rice, B. M.; Chabalowski, C. F.; Adams, G. F.; Mowrey, R. C.; Page, M. *Chem. Phys. Lett*. **1991**, *184*, 335.

(22) Raff, L. M.; *J. Chem. Phys*. **1989**, *90*, 6313.

(23) (a) Wodtke, A. M.; Hintsa, E. J.; Somorjai, J.; Lee, Y. T. *Isr. J. Chem*. **1989**, *29*, 383. (b) Wodtke, A. M.; Lee, Y. T. *J. Phys. Chem*. **1985**, *89*, 4744.

(24) Okabe, H. *J. Chem. Phys.* **1975**, *62*, 2782.

(25) Raff, L. M.; Thompson, D. L. "The Classical Trajectory Approach to Reactive Scattering" in *Theory of Chemical Reaction Dynamics*; Baer, M., Ed.; CRC Press: Boca Raton, FL, 1985, Vol. III, 1.

(26) Raff, L. M. *J. Chem. Phys*. **1988**, *89*, 5680; Raff, L. M. *J. Chem. Phys*. **1991**, *95*, 8901.

(27) Liu, D.; Letendre, L.; Dai, H.; Halpern, J. B.; Pibel, C. D. Private communication and *J. Chem. Phys.* (submitted for publication).

(28) Herzberg, G. *Spectra of Diatomic Molecules*; D. van Nostrand Co., Inc.: New York, 1950.

(29) (a) Holmes, B. E.; Setser, D. W. *J. Phys. Chem*. **1978**, *82*, 2450. Holmes, B. E.; Setser, D. W. *J. Phys. Chem.* **1978**, *82*, 2461 and (b) *Physical Chemistry of Fast Reactions*, Smith, I. W. M., Ed.; Plenum: New York, 1980, Vol. 2, p 83.